Table 3 Major toxicity findings for p-(α,α-dimethylbenzyl) phenol in the newborn and young rat main studies

	Newborn study (mg/kg)				Young study (mg/kg)			
	0	30	100	300	0	100	300	1000
Male								
Dead or moribund	0/12	0/12	0/12	0/12	0/14	0/7	0/7	3/14
ALT, γ-GTP	/	–	–	–	/	–	–	↑
BUN, Creatinine	/	–	–	–	/	–	–	↑
Relative liver weight	/	–	–	–	/	–	↑	↑
Relative kidney weight	/	–	–	↑	/	–	–	↑
Stomach, hyperplasia	0/6	0/6	0/6	0/6	0/7	0/7	0/7	1/6
Liver, proliferation bile ducts	0/6	0/6	0/6	0/6	0/7	0/7	0/7	6/6
Kidney, regeneration	0/6	0/6	0/6	0/6	3/7	3/7	5/7	6/6
Kidney, dilatation	0/6	0/6	1/6	6/6	0/7	0/7	0/7	6/6
Female								
Dead or moribund	0/12	0/12	0/12	0/12	0/14	0/7	0/7	1/14
ALT, γ-GTP	/	–	–	–	/	–	–	↑
BUN, Creatinine	/	–	–	↑,–	/	–	–	–
Relative liver weight	/	–	–	–	/	–	–	↑
Relative kidney weight	/	–	–	↑	/	–	–	↑
Stomach, hyperplasia	0/6	0/6	0/6	0/6	0/7	0/7	0/7	3/7
Liver, proliferation bile ducts	0/6	0/6	0/6	0/6	0/7	0/7	0/7	7/7
Kidney, regeneration	0/6	0/6	0/6	0/6	0/7	1/7	0/7	7/7
Kidney, dilatation	0/6	0/6	2/6	6/6	0/7	0/7	0/7	4/7

Only critical data are shown in this table. Data are numbers of animals with the change of the number examined. Slashes and bars mean no statistical significance as compared to controls. ↑ indicates significant increase at $P < 0.05$. Relative kidney weights were increased 2.5- and 2.1-fold for males and females at 300 mg/kg in the newborn study. For the young study, 14 males and 14 females (half for examination of recovery) were assigned to each group but 6 males and 7 females at 1000 mg/kg were re-assigned for 28-day examination because of deaths.

and 300 mg/kg. The absolute ovary weights were still lowered by 32% at 300 mg/kg after the recovery-maintenance period. Increased numbers of atretic follicles were found in ovaries of half of the females at 300 mg/kg at the end of the dosing period, and most females continued to show various changes such as decreased numbers of corpa luteua in the ovaries and hypertrophy of endometrial epithelium in the uteri, after the recovery-maintenance period.

In the young study, two males and one female died, and one male was killed in a moribund condition at 1000 mg/kg. The final body weights were reduced by 18%, limited to males. On urinalysis, both sexes showed irregularly sized particles of a black substance, accompanied by 2–4 fold elevation of urine volume. Clear changes of several biochemical parameters such as ALT, γ-GTP, BUN, and creatinine, increases of relative liver and kidney weights, and histopathological changes in the forestomach (squamous hyperplasia), liver (bile duct proliferation), and kidney (regeneration of tubular epithelium and dilatation of tubules) were also observed at 1000 mg/kg. A dose of 300 mg/kg was considered to cause slight toxicity, because the abnormal urinary contents described above were found in half of both sexes and a slightly elevated incidence of mild regeneration of the tubular epithelium was noted in male kidneys. After the two-week recovery period, the pathological changes in male kidneys at 1000 mg/kg continued to be evident. There were no signs of toxicity at 250 and 500 mg/kg in the dose-finding study although the administration period was only half and urinalysis and histopathological examinations were not performed.

The pNOAEL of 30 mg/kg/day for newborn rats is clear and one of 100 mg/kg/day for young rats is reasonable because of slight toxicity at 300 mg/kg in the main study and limited information at 250 mg/kg in the dose-finding study. Toxicity for newborn rats was evident at 300 mg/kg as all animals of both sexes showed histopathological changes in kidneys, with increased relative weights. However, the degree of toxicity for young rats at 1000 mg/kg was obviously much stronger than that of newborn rats at 300 mg/kg, which appeared to be equivalent to doses of 700–800 mg/kg in young rats. Therefore, pUETLs of 300 and 700–800 mg/kg/day may be appropriate for newborn and young rats, respectively. It should be specially noted that this chemical may have endocrine disrupting properties, especially against females, when given only during the suckling phase.

(Hydroxyphenyl)methyl phenol (Table 4)

The newborn investigation was conducted at doses of 0, 20, 60, and 200 mg/kg for dose-finding and 0, 16, 40, and 100 mg/kg for the main study. The young study was conducted at doses of 0, 100, 500, and 1000 mg/kg for dose-finding and 0, 8, 40, 200, and 1000 mg/kg for the main study.

Common changes were limited to depression of body weight and death at high doses in newborn and young rats. The highest dose of 100 mg/kg in the newborn main study did not cause any changes, but half the animals at 200 mg/kg in the newborn dose-finding study died, without accompanying liver weight changes in surviving

Table 4 Major toxicity findings for (hydroxyphenyl)methyl phenol in the newborn and young rat main studies

	Newborn study (mg/kg)			Young study (mg/kg)			
	0	100	200†	0	40	200	1000
Male							
Dead or moribund	0/12	0/12	3/6	0/12	0/12	0/12	0/12
Final body weight	/	–	↓	/	–	–	↓
Total cholesterol	/	–	↑	/	–	–	↓
Relative liver weight	/	–	–	/	–	–	↑
Stomach, hyperplasia	0/6	0/6	no data	0/6	0/6	0/6	6/6
Liver, centrilobular hypertrophy	0/6	0/6	no data	0/6	0/6	2/6	4/6
Female							
Dead or moribund	0/12	0/12	3/6	0/12	0/12	0/12	1/12
Final body weight	/	–	(↓)	/	–	–	(↓)
Total cholesterol	/	–	–	/	↓	↓	↓
Relative liver weight	/	–	–	/	–	↑	↑
Stomach, hyperplasia	0/6	0/6	no data	0/6	0/6	0/6	6/6
Liver, centrilobular hypertrophy	0/6	0/6	no data	0/6	0/6	0/6	4/6

Only critical data are shown in this table. † indicates a dose from the dose-finding study. Numbers are for animals with the feature in the total examined. Slashes and bars mean no statistical significance as compared with controls. ↑ indicates significant increase $P < 0.05$. ↓ indicates significant decrease at $P < 0.05$. () indicates that statistical significance was not obtained. Final body weights of surviving newborn males at 200 mg/kg in the dose-finding study were reduced by 30% (14% for females, not significant), respectively. Final body weights of young male rats at 1000 mg/kg in the main study were decreased by 11.8% (5.7% for females, not significant). Increase of relative liver weights was 13% in females at 200 mg/kg, and 16 and 27% in males and females at 1000 mg/kg in the young main study.

animals. There were no chemical-related changes with other examinations, including developmental parameters. In the young study, one female became moribund and the final body weights of males were decreased at 1000 mg/kg. All animals of both sexes at this dose showed squamous hyperplasia of the forestomach or limiting ridge with ulceration, and two-thirds of the animals featured centrilobular hypertrophy of hepatocytes with decrease of total cholesterol (29–51% drop) and increase of relative liver weight. At 200 mg/kg, low incidences of centrilobular hypertrophy in the livers of males and slight increase of liver weights in females with low total cholesterol (45% drop) were found. No toxicity was apparent at 40 mg/kg in the main study. No toxicity was also found at 100 mg/kg in the dose-finding study, but a histopathological examination was not conducted. There were no abnormalities on hematological examination and urinalysis at any dose.

The pNOAEL is considered to be 100 mg/kg/day for newborn rats and 40 mg/kg/day may be appropriate for young rats because of the limited information at 100 mg/kg in the dose-finding study. Although toxicity at 1000 mg/kg for young rats was evident, the dose inducing the same effects in newborn rats was clearly less than 200 mg/kg, because half of the animals died at this dose. We speculate that the dose range for one death in 12 newborn rats would be within 140–160 mg/kg. It is clear that the dose–response curve is much steeper for newborn than young rats. Based on our consideration, pUETLs of 140–160 and 1000 mg/kg/day may be equivalent for newborn and young rats, respectively.

Trityl chloride (Table 5)

The newborn investigation was conducted at doses of 0, 20, 60, 200, and 600 mg/kg for dose-finding and 0, 12, 60, and 300 mg/kg for the main study. The young investigation was conducted at doses of 0, 30, 100, 300, and 1000 mg/kg for dose-finding and 0, 12, 60 and 300 mg/kg for the main study.

Common effects were observed in livers of newborn and young rats. In the newborn study, increase of relative liver weights were shown at 60 mg/kg and more in both sexes and centrilobular hypertrophy of hepatocytes was noted in 300 mg/kg females. In the dose finding newborn study, one female died and increase of relative liver weights of both sexes at 600 mg/kg was more evident with low body weights (11.3% drop for males, 13.8% for females). There were no chemical-related changes with other examinations including developmental parameters. In the young study, both sexes at 60 mg/kg showed a high incidence of centrilobular hypertrophy of hypetocytes with limited increases of relative liver weights (10–14%). At 300 mg/kg, soft feces and mucosal thickening of cecum in most animals were observed in addition to more extensive hepatic changes. Although relative kidney weights were increased at 300 mg/kg in males and 60 and 300 mg/kg in females, there were no renal histopathological findings. Hematological and blood chemical examinations revealed several slight to moderate changes (56% as the maximum) in fibrinogen, ALT, total cholesterol and glucose, as well as prolongation of prothrombin and activated thromboplastin times, at 300 mg/kg.

pNOAELs of 60 and 12 mg/kg/day for newborn and young rats appear appropriate because of the lack of information at higher doses in the dose-finding study, which showed no toxicity but without histopathological examination. The dose of 300 mg/kg in the young main study was a clear toxic level, but intensity was much stronger than that at 300 mg/kg in the newborn main study while less that at 600 mg/kg in the dose-finding study. Based on these data, the toxicity with 300 mg/kg for young rats is considered to be within the range with 400–500 mg/kg for newborn rat

Table 5 Major toxicity findings for trityl chloride in the newborn and young rat main studies

	Newborn study (mg/kg)				Young study (mg/kg)			
	0	60	300	600†	0	12	60	300
Male								
Death	0/12	0/12	0/12	0/6	0/12	0/6	0/12	0/12
Final body weight	/	–	–	↓	/	–	–	↓
ALT, Total cholesterol	/	–	–	–	/	–	–	↑
Relative liver weight	/	↑	↑	↑	–	–	↑	↑
Relative kidney weight	/	–	–	–	–	–	–	↑
Cecum, thickening	0/6	0/6	0/6	no data	0/6	0/6	0/6	5/6
Liver, centrilobular hypertrophy	0/6	0/6	0/6	no data	0/6	0/6	3/6	6/6
Female								
Death	0/12	0/12	0/12	1/6	0/12	0/6	0/12	0/12
Final body weight	/	–	–	↓	/	–	–	–
ALT, Total cholesterol	/	–	–	–	/	–	–	-,↑
Relative liver weight	/	↑	↑	↑	–	–	↑	↑
Relative kidney weight	/	–	–	–	–	–	↑	↑
Cecum, thickening	0/6	0/6	0/6	no data	0/6	0/6	2/6	5/6
Liver, centrilobular hypertrophy	0/6	0/6	4/6	no data	0/6	0/6	5/6	6/6

Only critical data are shown in this table. †indicates a dose from the dose-finding study. Numbers are for animals with the feature in the total examined. Slashes and bars mean no statistical significance as compared to controls. ↑ indicates significant increase $P < 0.05$. ↓indicates significant decrease at $P < 0.05$. Relative liver weights were increased by 11% for males and 8% for females at 60 mg/kg, and 29% for both sexes at 300 mg/kg in the newborn main study and by 44% for males and 46% for females at 600 mg/kg in the newborn dose-finding study. Body weight depression in males (13%) and an increase of relative liver weights (32% for males, 40% for females) were observed at 300 mg/kg in the young main study.

Therefore, pUETLs of 400–500 and 300 mg/kg/day are proposed as appropriate for newborn and young rats, respectively.

1,3,5-Trihydroxybenzene (Table 6)

The newborn investigation was conducted at doses of 0, 100, 500, and 1000 mg/kg for dose-finding and at 0, 20, 100, and 500 mg/kg for the main study. The young investigation was conducted at doses of 0, 100, 250, 500, and 1000 mg/kg for dose-finding and at 0, 30, 100, 300, and 1000 mg/kg for the main study.

Common changes were observed in the thyroids and liver. The only toxic change in newborn main study was hypertrophy of thyroid follicular cells with increase in relative thyroid weights in both sexes at 500 mg/kg. Increased relative liver weights in females were not accompanied by any histopathological changes. Although decrease of adrenal weight and histopathological alterations such as vacuolization and pigmentation were noted at the end of the dosing and recovery-maintenance periods, these were always slight and not dose-dependent. There were no chemical-related changes with other examinations, including developmental parameters, in newborn rats. In the young study, similar effects on the thyroids and liver were found at 1000 mg/kg, but the incidence of thyroid histopathological changes was slightly less than in newborn animals at 500 mg/kg.

pNOAELs of 100 and 300 mg/kg/day for newborn and young rats can be considered appropriate because of the lack of data with dose settings between 100 to 500 mg/kg in the newborn, and no histopathological examination at 500 mg/kg in the young dose-finding study. The degree of toxicity at 1000 mg/kg for young rats was almost equal to that at 500 mg/kg for newborn rats. Therefore, pUETLs of 500 and 1000 mg/kg/day are proposed as equivalents for newborn and young rats, respectively.

DISCUSSION

More than 100 000 industrial chemicals are now in use around the world and sufficient toxicity information is available for only a small proportion. The Japanese government started the Existing Chemical Safety Program to obtain minimal toxicity data sets from 28-day toxicity studies using young rats for high production volume chemicals lacking toxicity information. For the present six targeted chemicals, we found toxicity information for only two chemicals by literature search. Daniel *et al.* (1993) reported no toxic effects of 2-chlorophenol on oral administration to male and female Sprague Dawley rats at up to 257 mg/kg for 10 days or 150 mg/kg for 90 days. Our results were consistent with their data, as we found no toxicity at 500 mg/kg in young dose-finding study (14 days administration) and at 200 mg/kg in the young study (28 days), while further providing information on CNS effects at higher doses. As for (hydroxyphenyl)methyl phenol, consisting of bisphenol D, E, and F isomers, bisphenol F has been reported to have estrogenic potential evidenced by several *in vitro* and *in vivo* experiments (Hashimoto *et al.* 2001; Yamasaki *et al.* 2002; Stroheker *et al.* 2003). However, we could not establish any such activity in this study. Our results are reasonable because oral administration of bisphenol F increased relative uterus weights only at more than 100 mg/kg, but not 50 mg/kg given during PNDs 22–25 (Stroheker *et al.* 2003), while our highest dose of (hydroxyphenyl)methyl phenol was equivalent to 30 mg/kg of bisphenol F.

Table 6 Major toxicity findings for 1,3,5-trihydroxybenzene in the newborn and young rat main studies

	Newborn study (mg/kg)			Young study (mg/kg)		
	0	100	500	0	300	1000
Male						
Relative organ weight						
Liver	/	–	–	/	–	↑
Thyroids	/	–	↑	/	–	(↑)
Histopathology						
Liver	0/6	0/6	0/6	0/6	0/6	0/6
Thyroids, hypertrophy	0/6	0/6	4/6	0/6	0/6	2/6
Female						
Relative organ weight						
Liver	/	–	↑	/	–	↑
Thyroids	/	–	(↑)	/	–	(↑)
Histopathology						
Liver	0/6	0/6	0/6	0/6	0/6	0/6
Thyroids, hypertrophy	0/6	0/6	5/6	0/6	0/6	4/6

Only critical data are shown in this table. Slashes and bars mean no statistical significance as compared with controls. ↑ indicates significant increase $P < 0.05$ (except in parentheses where statistical significance was not attained). Numbers are for animals with the feature in the total examined. Increase of relative organ weights at 500 mg/kg in the newborn main study was observed for thyroids (39% for males, 24% for females) and liver (9% for females). Increase of relative organ weights at 1000 mg/kg in the young main study was observed for thyroids (14% for males, 19% for females) and liver (23% for males and 9% for females).

Table 7 Comparative susceptibility of newborn and young rats to the six chemicals

	Newborn study		Young study		pNOAEL	pUETL
	pNOAEL	pUETL	pNOAEL	pUETL	Young/Newborn	Young/Newborn
	mg/kg/day		mg/kg/day			
2-Chlorophenol	40	200–250	200	1000	5.0	4.0–5.0
4-Chlorophenol	100	300	100	500	1.0	1.7
p-(α,α-Dimethylbenzyl) phenol	30	300	100	700–800	3.3	2.3–2.7
(Hydroxyphenyl) methyl phenol	100	140–160	40	1000	0.4	6.3–7.1
Trityl chloride	60	400–500	12	300	0.2	0.6–0.8
1,3,5-Trihydroxybenzene	100	500	300	1000	3.0	2.0

Although there has been no reports for p-(α,α-dimethylbenzyl) phenol, it causes endocrine disruption and possible antiestrogenic activity, when administered to newborn female rats in this study. Therefore, further studies on this chemical should be conducted to elucidate the mechanisms, because the present investigation did not indicate any effects on sexual differentiation such as preputial separation, vaginal opening and the estrous cycle.

For our focus on the comparative sensitivity of newborn and young rats to chemicals, two toxicity endpoints, pNOAEL and pUETL, were newly defined as appropriate, considering the entire data sets from both main and dose-finding studies. We believe that this alternative assessment approach allowed us to make more realistic comparisons between newborn and young rats under the same experimental conditions as far as possible.

The ratios of pNOAELs for chemicals between newborn and young rats may provide an additional UF value in risk assessment according to susceptibility of newborn rats, because regulatory limit values for chemicals to protect public health of humans, including infants, are derived from the division of NOAEL by UFs. The data in Table 7 indicate newborn rats to be 1–5 times more susceptible to four of the tested chemicals, 2- and 4-chlorophenols, p-(α,α-dimethylbenzyl) phenol and 1,3,5-trihydroxybenzene, than young rats in terms of the pNOAELs, similar to the results of previous analyzes of five phenolic chemicals, 4-nitro-, 2,4-dinitro-, 2,4,6-trinitro-, 3-methyl- and 3-amino-phenols (Koizumi *et al.* 2001, 2002, 2003; Takahashi *et al.* 2004). Immaturity in the detoxification potential of phase 1 and phase 2 enzymes in newborn animals may be the major cause of higher toxicity in newborn rats (Rich & Boobis 1997; Gow *et al.* 2001), because these chemical classes are probably direct toxicants. In the case of (hydroxyphenyl)methyl phenol, the pNOAEL (100 mg/kg/day) for newborn rats was 2.5 times higher than that (40 mg/kg/day) for young rats, but it can be speculated that values are in practice rather similar because the toxicity for young rats at the high dose, 200 mg/kg, was only slight (Table 4). As for trityl chloride, newborn rats were obviously less susceptible (0.2 for the pNOAEL ratio). Similar results were

also reported from our previous analysis for bromoalkanes (Hirata-Koizumi *et al.* 2005) and may be explained by mechanisms of action and metabolic characteristics of newborn rats. As this class of chemicals possibly requires metabolism to act as toxicants, the relatively mature metabolic enzyme status of young rats would be expected to provide toxic intermediates by metabolic activation to a greater extent than in newborn rats, as evidenced by data for previously reported chemicals (Onkenhout *et al.* 1986; Kennedy *et al.* 1993). Other compounds such as acetaminophen, bromobenzene, and carbon tetrachloride have also been shown to not produce liver injury in neonatal animals at doses that are hepatotoxic to adults (Gregus & Klaassen 1998).

The ratios of pUETLs, doses inducing the same degree of toxicity in newborn and young rats, were almost the same as for pNOAELs with the direct toxicants, as shown in Table 7. However, newborn rats were considerably more susceptible to (hydroxyphenyl)methyl phenol when considering the pUETL, due to the much steeper dose–response curve in newborn rats, with a 100 mg/kg/day pNOAEL and half the animals dying at 200 mg/kg, compared with a 40 mg/kg/day pNOAEL and only one death in 12 animals at 1000 mg/kg for young rats. Although young rats showed stomach hyperplasia in addition to hepatotoxicity at 1000 mg/kg, the cause of newborn deaths at 200 mg/kg was unclear. With regard to trityl chloride, the pUETL for young rats was almost the same as for newborn although the latter were less susceptible. Such an anomaly has also been found for bromoalkanes previously analyzed. Another example of a chemical for which susceptibility differs at low and high doses is chlorpyrifos, the maximum tolerated dose in 17-day-old rats being reported to be five times less than that in adults following oral exposure (Moser & Padilla 1998), but the differential sensitivity not appearing in low-dose exposure (Pope & Liu 1997). Thus as there are several chemicals of which dose–response curve in newborn rats was obviously steeper than that in young rats, pUETL ratios should be also taken into account for the susceptibility of newborn rats as the second endpoint marker.

In conclusion, newborn rats were 2–5 times more susceptible than young rats in terms of both the pNOAEL and the pUETL in most cases. One exception was that young rats were clearly more susceptible than their newborn counterparts for trityl chloride.

ACKNOWLEDGMENT

The authors gratefully acknowledge the financial support of the Office of Chemical Safety, Pharmaceutical and Medical Safety Bureau, Ministry of Health, Labor and Welfare, Japan and also deeply appreciate the efforts of the six Japanese contract laboratories in performing the actual animal toxicity studies.

REFERENCES

Bartlett MS (1937) Properties of sufficiency and statistical tests. *P Roy Soc Lond A Mat* **160**: 268–282.

Chemical Products' Handbook (2004) *Chemical Products of 14504 '14504 no Kagakushohin'*. The Chemical Daily, Tokyo (in Japanese).

Daniel FB, Robinson M, Olson GR, York RG, Condie LW (1993) Ten and ninety-day toxicity studies of 2-chlorophenol in Sprague-Dawley rats. *Drug Chem Toxicol* **16**: 277–291.

Dourson M, Charnley G, Scheuplein R (2002) Differential sensitivity of children and adults to chemical toxicity. II. Risk and regulation. *Regul Toxicol Pharmacol* **35**: 448–467.

Dunnett CW (1964) New tables for multiple comparisons with a control. *Biometrics* **20**: 482–491.

Fisher RA (1973) *Statistical Methods for Research Workers*, 14th edn. Hafner Publishing Co, New York.

Fukuda N, Ito Y, Yamaguchi M *et al.* (2004) Unexpected nephrotoxicity induced by tetrabromobisphenol A in newborn rats. *Toxicol Lett* **150**: 145–155.

Gow PJ, Ghabrial H, Smallwood RA, Morgan DJ, Ching MS (2001) Neonatal hepatic drug elimination. *Pharmacol Toxicol* **88**: 3–15.

Gregus Z, Klaassen CD (1998) Hepatic disposition of xenobiotics during prenatal and postnatal development. In: Polin RA, Fox WF, (eds). *Fetal and Neonatal Physiology*. Saunders, Philadelphia, pp. 1472–1493.

Hasegawa R, Koizumi M, Hirose A (2004) Principles of risk assessment for determining the safety of chemicals: Recent assessment of residual solvents in drugs and di (2-ethylhexyl) phthalate. *Congenit Anom Kyoto* **44**: 51–59.

Hashimoto Y, Moriguchi Y, Oshima H, Kawaguchi M, Miyazaki K, Nakamura M (2001) Measurement of estrogenic activity of chemicals for the development of new dental polymers. *Toxicol In Vitro* **15**: 421–425.

Hirata-Koizumi M, Kusuoka O, Nishimura N *et al.* (2005) Susceptibility of newborn rats to hepatotoxicity of 1,3-dibromopropane and 1,1,2,2-tetrabromomethane, compared with young rats. *J Toxicol Sci* **30**: 29–42.

Hollander M, Wolfe DA (1973) *Nonparametric Statistical Methods*. John Wiley and Sons, New York.

IPCS (International Programme on Chemical Safety) (2002) *Global Assessment of the State-of-the-Science of Endocrine Disruptors*. Damstra T, Barlow S, Bergman A, Kavlock R, van der Kraak G (eds). World Health Organization, Geneva.

Kennedy CH, Cohen KB, Bechtold WE *et al.* (1993) Effect of dose on the metabolism of 1,1,2,2-tetrabromoethane in F344/N rats after gavage administration. *Toxicol Appl Pharmacol* **119**: 23–33.

Koizumi M, Nishimura N, Enami T *et al.* (2002) Comparative toxicity study of 3-aminophenol in newborn and young rats. *J Toxicol Sci* **27**: 411–421.

Koizumi M, Noda A, Ito Y *et al.* (2003) Higher susceptibility of newborn than young rats to 3-methylphenol. *J Toxicol Sci* **28**: 59–70.

Koizumi M, Yamamoto Y, Ito Y *et al.* (2001) Comparative study of the toxicity of 4-nitrophenol and 2,4-dinitrophenol in newborn and young rats. *J Toxicol Sci* **26**: 299–311.

Landrigan PJ, Kimmel CA, Correa A, Eskenazi B (2004) Children's health and the environment: Public health issues and challenges for risk assessment. *Environ Health Perspect* **112**: 257–265.

Lee PC (1998) Disruption of male reproductive tract development by administration of the xenoestrogen, nonylphenol, to male newborn rats. *Endocrine* **9**: 105–111.

Mann HB, Whitney DR (1947) On a test of whether one of two random variables is stochastically larger than the other. *Ann Math Stat* **18**: 50–60.

Moser VC, Padilla S (1998) Age- and gender-related differences in the time course of behavioral and biochemical effects produced by oral chlorpyrifos in rats. *Toxicol Appl Pharmacol* **149**: 107–119.

Onkenhout W, Van Bergen EJ, Van der Wart JH, Vos GP, Buijs W, Vermeulen NP (1986) Identification and quantitative determination of four different mercapturic acids formed from 1,3-dibromopropane and its 1,1,3,3-tetradeutero analogue by the rat. *Xenobiotica* **16**: 21–33.

Pope CN, Liu J (1997) Age-related differences in sensitivity to organophosphorus pesticides. *Environ Toxicol Pharmacol* **4**: 309–314.

Rich KJ, Boobis AR (1997) Expression and inducibility of P450 enzymes during liver ontogeny. *Microsc Res Tech* **39**: 424–435.

Steel RD (1959) A multiple comparison rank sum test: Treatment versus control. *Biometrics* **15**: 560–572.

Stroheker T, Chagnon MC, Pinnert MF, Berges R, Canivenc-Lavier MC (2003) Estrogenic effects of food wrap packaging xenoestrogens and flavonoids in female Wistar rats: A comparative study. *Reprod Toxicol* **17**: 421–432.

Takahashi M, Ogata H, Izumi H *et al.* (2004) Comparative study of toxicity of 2,4,6-trinitrophenol (picric acid) in newborn and young rats. *Congenit Anom Kyoto* **44**: 204–214.

Takahashi O, Oishi S (2001) Testicular toxicity of dietary 2,2-bis (4-hydroxyphenyl) propane (bisphenol A) in F344 rats. *Arch Toxicol* **75**: 42–51.

Yamasaki K, Takeyoshi M, Yakabe Y *et al.* (2002) Comparison of reporter gene assay and immature rat uterotrophic assay of twenty-three chemicals. *Toxicology* **170**: 21–30.

Tbx6-mediated Notch signaling controls somite-specific *Mesp2* expression

Yukuto Yasuhiko*, Seiki Haraguchi†, Satoshi Kitajima*, Yu Takahashi*, Jun Kanno*, and Yumiko Saga‡§

*Cellular and Molecular Toxicology Division, National Institute of Health Sciences, Kamiyoga 1-18-1, Setagaya-ku, Tokyo 158-8501, Japan; †The Wellcome Trust/Cancer Research UK Gurdon Institute, University of Cambridge, Cambridge CB2 1QN, United Kingdom; and ‡Division of Mammalian Development, National Institute of Genetics, Mishima, Shizuoka 411-8540, Japan

Edited by Kathryn V. Anderson, Sloan–Kettering Institute, New York, NY, and approved January 10, 2006 (received for review September 21, 2005)

Mesp2 is a transcription factor that plays fundamental roles in somitogenesis, and its expression is strictly restricted to the anterior presomitic mesoderm just before segment border formation. The transcriptional on–off cycle is linked to the segmentation clock. In our current study, we show that a T-box transcription factor, Tbx6, is essential for *Mesp2* expression. Tbx6 directly binds to the *Mesp2* gene upstream region and mediates Notch signaling, and subsequent *Mesp2* transcription, in the anterior presomitic mesoderm. Our data therefore reveal that a mechanism, via Tbx6-dependent Notch signaling, acts on the transcriptional regulation of *Mesp2*. This finding uncovers an additional component of the interacting network of various signaling pathways that are involved in somitogenesis.

enhancer | transgenic mouse | RBPJκ | luciferase assay

Somitogenesis not only is an important morphogenic process that generates metameric structures in vertebrates, but it is also a intriguing model system for the study of the interactions among various signaling cascades that facilitate periodic pattern formation. The segmental boundary of each somite forms at the anterior end of the presomitic mesoderm (PSM) or unsegmented paraxial mesoderm, which is supplied from the primitive streak or tailbud at a later stage of development.

Notch signaling plays fundamental roles in segmental pattern formation by means of oscillating the activity in the tailbud, its forward movement through the PSM as traveling waves, and its stabilization at the anterior end of the PSM (1, 2). A segment border forms at the posterior limit of the stabilized stripe of Notch signaling activity (2). The oscillation of the Notch signals in the tailbud region is regulated by the transcription factor Hes7 (3), a glycosyltransferase Lunatic fringe (2), and by Wnt signaling (4). In contrast, the positioning of segment formation by a determination wavefront is thought to be defined by antagonistic interactions between gradients of Fgf signals from the posterior end (5) and retinoic acid (RA) from anterior end of the PSM (6). On the other hand, mutant analyses identified a T-box protein, Tbx6, as an indispensable component for correct PSM differentiation and segmentation (7). However, the direct molecular relationships between these factors have not yet been well characterized.

A basic helix–loop–helix transcription factor, Mesp2, has a crucial role both in somite segment border formation and in the establishment of the rostrocaudal patterning of each somite (8). *Mesp2* shows dynamic and periodical expression in the anterior PSM, which defines the positioning of the forming somite by suppressing Notch signaling, partly through the activation of *lunatic fringe* (2). Genetic analyses have revealed that *Mesp2* expression itself is controlled by Notch signaling, which indicates the presence of a complicated feedback circuitry (9, 10). However, the molecular mechanisms that control *Mesp2* expression remain largely unknown. In our present study, we show that Tbx6 directly binds to upstream elements of the *Mesp2* gene and is essential for the activation of *Mesp2* expression. Furthermore, we demonstrate that Notch signaling strongly enhances *Mesp2* activation by Tbx6, and we identify the sequences that are important for this enhancement. Hence, we identify a Tbx6-mediated Notch signaling pathway as a mechanism underlying the regulation of *Mesp2* expression.

Results and Discussion

Evolutionally Conserved Sites in the Upstream Region of the *Mesp2* Gene Promote Strong Reporter Activity in Forming Somites. The distinct expression patterns of *Mesp2* expression during somitogenesis are strictly regulated. As we previously reported (11), a transgenic approach has revealed that a 300-bp portion of the 5′-adjoining sequence of the *Mesp2* ORF induces lacZ reporter activity in forming somites. This finding reflects the *Mesp2* expression pattern in the anteriormost PSM, suggesting that this 5′ region includes cis elements that regulate PSM-specific *Mesp2* expression. We performed comparisons of the genomic sequences of mouse *Mesp2* and its putative ortholog in zebrafish, *mespb*, and identified five conserved sites (A–E) in this 300-bp segment (Fig. 1*A*). Each of these sites was then independently examined for enhancer properties by using a transgenic strategy. We previously showed that one of our transgenic constructs, *P2L-100*, containing sites D and E, which cover the 100 bp upstream of the *Mesp2* ATG start codon, did not activate the lacZ reporter gene (11). We thus concentrated our analysis on sites A–C in our current experiments by ligating them with the *P2L-100* construct. None of these three sites could individually promote lacZ reporter activity in somites (Fig. 1*B*). However, the combination of sites A and B (designated as "site A+B" hereafter) induced strong β-gal expression in the somite region (Fig. 1*B Left*). This result suggests that specific transcription factors required for somite-specific *Mesp2* expression may bind to site A+B.

Tbx6 Binds to Cis-Regulatory Elements of the *Mesp2* Gene and Activates Its Expression. To identify transcription factors that bind to the cis-regulatory elements of the *Mesp2* gene, we performed yeast one-hybrid screening. Using site A+B sequences as the "bait," we isolated a T-box transcription factor, Tbx6, as a candidate binding protein. T-box proteins have been shown to recognize and bind to nucleotide sequences of 10–11 bp in length that possess a conserved CACAC motif (12). Significantly, sites A, B, and D in the upstream sequences of the *Mesp2* gene contain this motif (Fig. 2*A*). EMSA subsequently revealed that FLAG-Tbx6 binds to both site B and site D, in addition to the T (Brachyury) binding consensus sequence (12) (Fig. 6*A*, which is published as supporting information on the PNAS web site). By using site B sequences as a probe for FLAG-Tbx6 binding, EMSA experiments produced two band shifts, a distinct band

Conflict of interest statement: No conflicts declared.

This paper was submitted directly (Track II) to the PNAS office.

Abbreviations: PSM, presomitic mesoderm; NICD, Notch intracellular domain; RA, retinoic acid.

§To whom correspondence should be addressed. E-mail: ysaga@lab.nig.ac.jp.

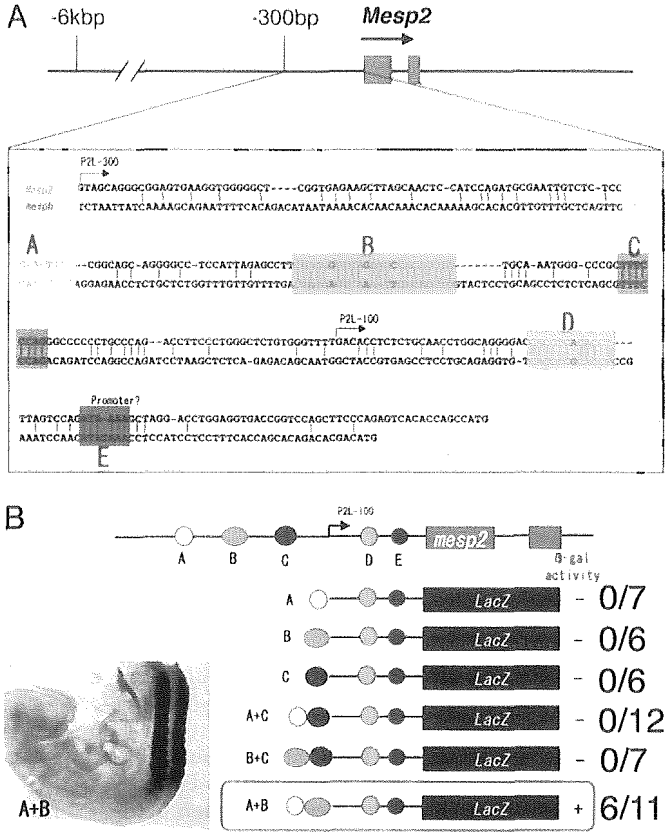

Fig. 1. Characterization of the *Mesp2* enhancer region. (*A*) Comparisons between the genomic sequences of mouse *Mesp2* and zebrafish *mespb* (an ortholog of mouse *Mesp2*) reveal five conserved sites in the 300-bp proximal promoter region. These conserved sites are denoted as A–E. The numbers above the genomic sequences indicate the base count from the ATG transcriptional start site of the *Mesp2* ORF. (*B*) Summary of the transient transgenic assay results with different combinations of conserved sites from the *Mesp2* upstream region (sites A–C). Each site was tested either alone or in combination with other sites for somite-specific enhancer activity. The presence (+) or absence ( ) of β-gal activity and the incidence of this among transgene-positive embryos is shown schematically on the right of each reporter construct. The combination of site A and site B (shown as A + B) resulted in strong somite-specific enhancer activity (*Left*).

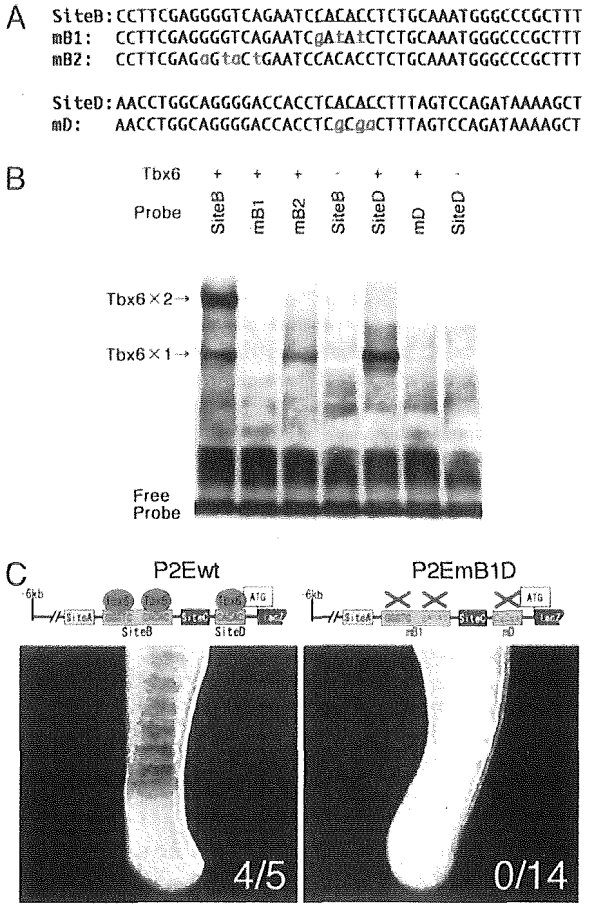

Fig. 2. Tbx6 binds to the *Mesp2* enhancer and promotes gene expression. (*A*) Wild-type and mutant sequences of site B and site D. The bases highlighted in lowercase denote the mutation sites. (*B*) Tbx6 binds to site B and site D. Digoxigenin-labeled oligonucleotide probes containing site B or site D were subjected to EMSA with (+) and without ( ) Tbx6. Mutation of the CACAC motif in site B (lane mB1) resulted in the loss of both the wild-type band shifts, whereas mutations in GGGTC (lane mB2) abolished only the upper band. Mutations in the CACAC motif from site D also eliminated the band shift (lane mD). (*C*) β-Gal reporter expression analysis in transgenic mouse embryos with constructs containing either wild-type or mutated *Mesp2* upstream regions. Each of the images is a lateral view with the anterior region toward the top. The numbers of β-gal-positive transgenic embryos are shown in each image (β-gal-positive/transgene-positive).

with a lower mobility and a weaker band with a higher mobility. These two species presumably represent the binding of two and one Tbx6 molecule(s), respectively, because palindromic repeats or spaced tandem repeats of two half fragments of site B generated band shift patterns identical to those of site B (Fig. 6*B*). Tbx6 binding to site B and site D was successfully competed for by oligonucleotides containing the T binding consensus sequence and could be supershifted by incubation of the forming complexes with an anti-FLAG antibody (Fig. 6*A*). We conclude therefore that Tbx6 binds to the upstream region of the *Mesp2* gene by means of the DNA binding activity of its T-box domain.

We next introduced nucleotide substitutions to the conserved CACAC motifs in sites B and D and examined the binding ability of Tbx6 to these mutated oligonucleotide probes. Interestingly, a mutation in site B, designated mB1 (Fig. 2*A*), eliminated both of the wild-type site B band shifts in an EMSA (Fig. 2*B*). Because T-box transcription factors can recognize palindromic sequences and bind to these sites as dimers (13, 14), we introduced nucleotide substitutions to the GGGTC sequence in site B, which is situated in the 5′ region adjacent to the CACAC motif (Fig. 2*A*, mB2). In subsequent EMSA analysis, the mB2 substitution was found to have eliminated only the upper site B band shift, indicating that this mutant oligonucleotide can bind only one Tbx6 molecule (Fig. 2*B*). These results suggest that site B is a partial palindrome that associates with two Tbx6 molecules and that the initial binding depends on the CACAC motif. The site D probe generated one EMSA band, and mutation of the CACAC motif in this site (mD) eliminated this band shift (Fig. 2*B*).

T-box proteins constitute a large family of transcription factors (15). *Tbx18* (16) and *Brachyury* (*Bra*) (17) are expressed in segmented somites and in the tailbud, respectively. Mga is a ubiquitous transcriptional repressor that possesses both T-box and basic helix–loop–helix motifs (18), and the T-box motifs of Mga and Tbx6 show similarities (19). In our present experiments, we examined the DNA-binding abilities of Tbx6, Bra, Mga, and Tbx18 to upstream *Mesp2* sequences using EMSA experiments (Fig. 6*D*). Bra and Tbx18 showed no binding activity to either site B or site D, whereas Mga bound weakly to site B. Taken together, we conclude from these data that Tbx6 is the most likely factor, among the T-box-containing proteins expressed in the PSM, that binds to site B and site D of the *Mesp2* gene.

To examine the function of these upstream *Mesp2* cis elements on gene expression, we performed transient transgenic mouse analyses using a lacZ reporter with mutated cis elements in 6-kb upstream sequences of the *Mesp2* ORF. The nucleotide substitutions that eliminate the binding of Tbx6 to sites B and D of the *Mesp2* promoter (P2EmB1D) diminished gene reporter activity in these assays (Fig. 2*C*). Furthermore, targeted disruption of sites B and D eliminated *Mesp2* expression in the forming somites of homozygous embryos (data not shown), demonstrating that these cis-regulatory elements are essential for somite-specific *Mesp2* expression.

In mouse embryo, *Mesp2* mRNA emerges in anterior PSM, at the position of S-1 (8, 9). Tbx6 protein exists also in S-1 (20). *Mesp2* is not expressed in the PSM of *Tbx6*-null mouse embryos (7), suggesting that it is a downstream target of Tbx6. Although the distinct *Mesp2* signal overlaps only in the anteriormost part of *Tbx6*, the initial *Mesp2* mRNA emerges in the more posterior region, overlapping with the *Tbx6* signal (Fig. 6*E*). These results suggest that Tbx6 is necessary at least for initiation of *Mesp2* expression.

In zebrafish, *fused somite* (*fss*), which encodes *Tbx24*, is known as a distant homolog of mouse *Tbx6*, and the corresponding mutant embryos have neither segmented somite nor *mespb* expression (21). The cis-regulatory elements are also well conserved between the upstream regions of *Mesp2* and *mespb* (Fig. 1*A*), and Tbx24 also binds to the *Mesp2* upstream region (data not shown). Recently, Davidson *et al.* (22) reported that, during heart development in the simple chordate *Ciona intestinalis*, a *Mesp* homolog is also expressed in a Tbx6-dependent manner. Comparing genomic sequences among *Ciona*, mouse, and zebrafish, the authors identified multiple Tbx6 binding sites in the upstream sequence of *Ciona Mesp* homolog. Taken together, we speculate from these findings that Tbx6-mediated activation of the *Mesp* genes is an evolutionally conserved mechanism in Chordata.

The Notch Intracellular Domain (NICD) Activates a *Mesp2* Reporter Construct in a Tbx6-Dependent Manner. To analyze the detailed regulatory mechanisms underlying the control of *Mesp2* expression, we constructed a *Mesp2* reporter system comprising a firefly luciferase reporter and *Mesp2* cis elements. Cotransfection of a Tbx6 expression vector with the *Mesp2* reporter increased luciferase activity by 10-fold (Fig. 3), indicating that Tbx6 functions as a transcriptional activator of *Mesp2*. In somite-stage embryos, *Tbx6* is expressed throughout the PSM and also in the tailbud region (20, 23), whereas *Mesp2* expression is restricted to the anterior PSM just before somite formation, and the expression overlaps only in the anterior limit of the *Tbx6* expression domain (Fig. 6*E*). The discrepancy between these expression patterns strongly indicates that other unknown factor(s) participate in the pathways that restrict the *Mesp2* expression domain to the anterior PSM. Because Notch signaling plays crucial roles in many aspects of somitogenesis, and given that *Mesp2* expression is known to depend on Dll1-Notch signaling (10), we examined the involvement of Notch signaling in the Tbx6-mediated transactivation of *Mesp2*.

The typical Notch signaling pathway is composed of ligands known as DSL (Delta, Serrate, and Lag-2), Notch receptors, effectors known as CSL (CBF-1, Suppressor of Hairless, and Lag-1), and a number of other proteins that modulate the functions of each component of the pathway (24). Once the DSL ligands bind to the Notch receptor, the NICD is proteolytically cleaved, translocates into the nucleus, and binds to its CSL effector (RBPJκ in the case of mouse) to activate the transcription of downstream target genes (24). We transiently introduced expression vectors for NICD and RBPJκ-VP16 (dominant-active RBPJκ) (25), in conjunction with Tbx6, into cultured cells bearing the *Mesp2* reporter. As a positive control, we used the

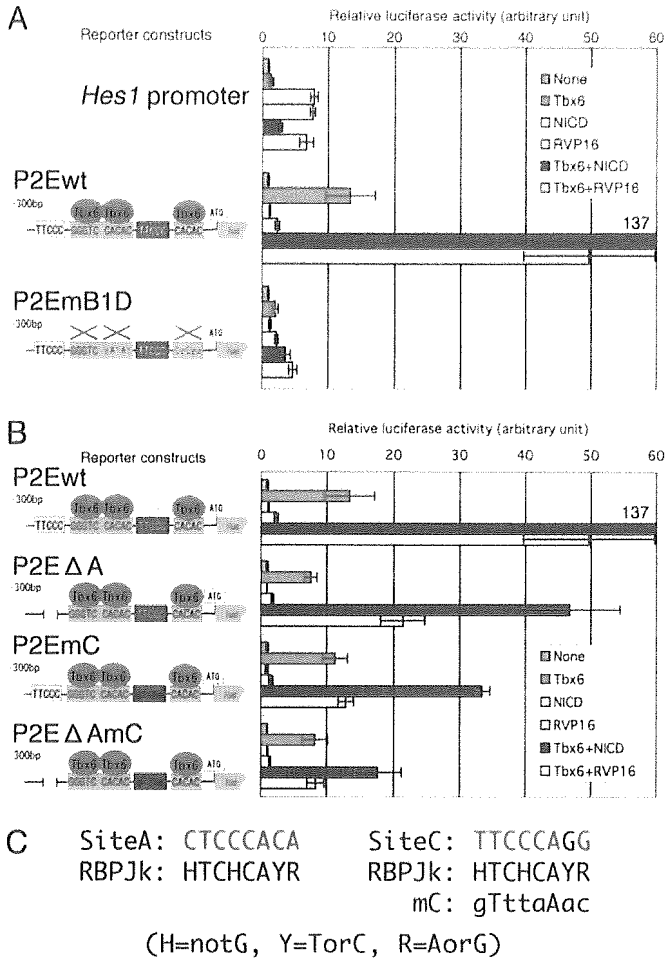

Fig. 3. *Mesp2* expression is activated by Notch signaling in a Tbx6-dependent manner. For each set of analyses, the luciferase activity was normalized to the values obtained in the absence of an expression vector (None). Error bars represent the standard deviation from six independent experiments. RVP16, RBPJκ-VP16. (*A*) Tbx6 activates a *Mesp2*–luciferase reporter gene construct synergistically with the NICD or RBPJκ-VP16. Mutation of site B and site D (denoted as P2EmB1D) eliminates this transactivation. (*B*) Notch signal activates the *Mesp2* reporter construct via site A and site C. The reporter constructs are indicated to the left of the graph. (*C*) Nucleotide sequences of the possible RBPJκ binding sites in site A (*Left*) and site C (*Right*) and the comparison between these regions and the RBPJκ binding consensus sequence (denoted as RBPJk) (27). The nucleotides matching the consensus sequence are shown in red for site A and site C. Nucleotide substitutions in site C (denoted as mC) are indicated in lowercase.

Hes1 promoter, which is known to be a downstream target of Notch signaling (26). Transfection of the *Hes1* reporter construct produced significant luciferase activity even in the absence of NICD (data not shown), reflecting the endogenous NICD activity, and the reporter activity increased further in the presence of either NICD or RBPJκ-VP16. In contrast, neither NICD nor RBPJκ-VP16 was found to activate the *Mesp2* reporter (Fig. 3*A*). However, when NICD and Tbx6 were cotransfected, significant increases in luciferase activity were detected (Fig. 3*A*). RBPJκ-VP16 also can activate the *Mesp2* promoter when cotransfected with *Tbx6* (Fig. 3*A*), suggesting that RBPJκ-dependent Notch signaling activated *Mesp2* reporter in a Tbx6-dependent manner. Consistent with this finding, mutations in site B and site D, which eliminate Tbx6 binding to the *Mesp2* upstream region, greatly reduced *Mesp2* reporter activation by NICD or RBPJκ-VP16 (Fig. 3*A*).

To identify the Notch signaling responsive site within the

DEVELOPMENTAL

Mesp2 upstream region, we analyzed the activity of two additional reporter constructs bearing either a deletion or a mutation in the conserved sites A and C, because these regions contain sequences that have some similarity to the RBPJκ consensus binding site (24, 27) (Fig. 3*C*). We speculated that these sites may play an important role in the regulation of *Mesp2* expression based on our observation that site A is essential for somite-specific expression in combination with site B (Fig. 1). Moreover, reporter activity in forming somites is lost when sequential deletion of the upstream region of the *Mesp2* gene removes a part of site C (11). In our current experiments, the deletion of site A reduced the levels of synergistic activation of the *Mesp2* reporter by both Notch signaling and Tbx6 by up to 50% (Fig. 3*B*, P2EΔA). Reporter activation was also remarkably diminished when we introduced mutations into both site A and site C (Fig. 3*B*, P2EΔAmC), suggesting that the binding of RBPJκ is required for the Tbx6-dependent transduction of Notch signaling. In contrast to the *Hes* family genes, no direct interaction between the Notch signaling pathway and the *Mesp2* regulatory region had been previously identified. Our current findings thus provide the first evidence that *Mesp2* is a direct target of Notch signaling. Furthermore, we identified a regulatory mechanism underlying the Notch signaling pathway that is based on the binding of Tbx6 to transcriptional regulatory sequences (summarized in Fig. 4 *A* and *B*).

We next conducted transient transgenic assays using our lacZ reporters with mutations in sites A and C. Surprisingly, the coexistence of the site A deletion and site C mutation (P2EΔAmC) in our reporter system showed somite-specific β-gal expression, although the activity was slightly weaker than normal (Fig. 5*A*). One possibility that might explain this disparity is that there may be a redundant, RBPJκ-independent pathway of Notch signaling that activates *Mesp2* expression. Consistent with this hypothesis, the P2EΔAmC reporter retained the ability to respond to the coexpression of NICD and Tbx6, although this activity was only 13% of wild-type levels (Fig. 3*B*). Notably, the P2EΔAmC reporter showed no synergistic activation after the coexpression of Tbx6 and RBPJκ-VP16 (Fig. 3*B*), indicating that the ability to respond to RBPJκ-dependent Notch signaling is eliminated by the disruption of sites A and C. These results suggest that Notch signaling activates *Mesp2* expression in both RBPJκ-dependent and RBPJκ-independent manners (Fig. 4*C*). Although most of the Notch signals are mediated by CSL effectors, such as RBPJκ, there is some reported evidence that suggests the existence of RBPJκ-independent Notch signal transduction pathways (28, 29). The molecular components involved in RBPJκ-independent Notch signaling are still poorly understood, but our present data suggest the possibility that Tbx6 not only facilitates RBPJκ-dependent Notch signaling but also acts as a component of an RBPJκ-independent Notch signaling pathway.

Another possible mechanism of somite-specific reporter expression that we observed in our P2EΔAmC transgenic embryos is the involvement of Notch-independent signals (Fig. 4*C*). Although it is clear that Notch signaling is genetically upstream of *Mesp2* activation (9, 10), *Psen1* knockout mouse embryos, which are deficient in Notch proteolysis and therefore do not produce NICD (30), show only moderate decreases in *Mesp2* expression levels (10). Together with our present findings, these observations may indicate that the controlling mechanism for *Mesp2* gene expression is a redundant and robust system and is composed of a number of signaling cascades. Regardless of this possibility, Tbx6 is likely to be essential for all of the signaling pathways involved in *Mesp2* expression, because mutation of the Tbx6 binding sites in the upstream regions of the *Mesp2* gene completely eliminates reporter expression in forming somites (Fig. 2*C*).

Because Tbx6 mRNA (Fig. 6*E*) and protein (20) are distributed throughout the tailbud and posterior PSM, the factors that restrict the expression domain of *Mesp2* in anterior PSM remain to be identified. Notably, although Tbx6 seems to activate reporter expression in cultured cells by itself, dominant-negative RBPJκ(R218H), which retains NICD binding activity but has lost any DNA binding ability (31), inhibits the Tbx6-dependent reporter activation by 50% (Fig. 5*B*). This finding suggests that

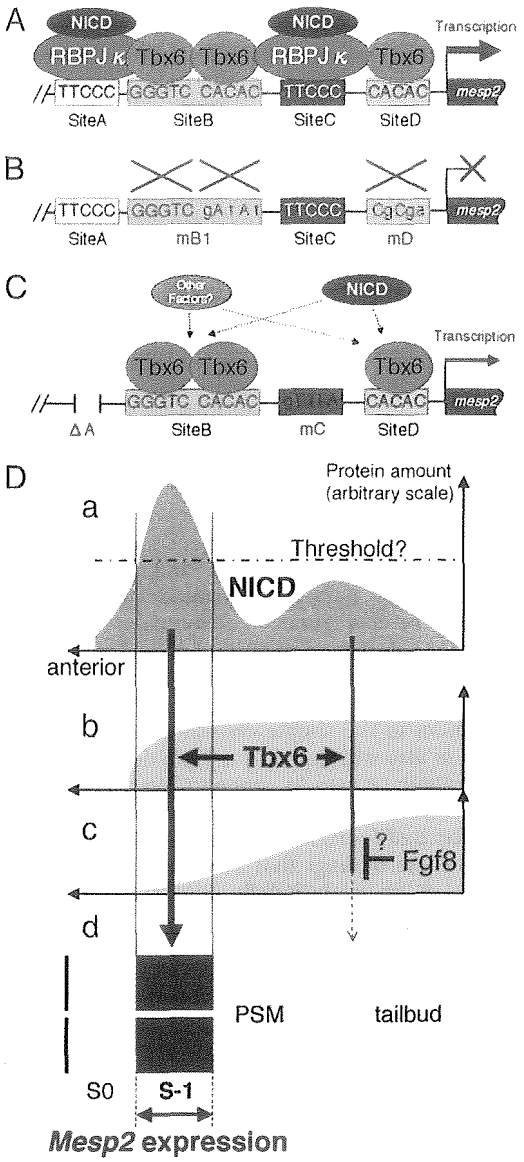

Fig. 4. Proposed mechanisms underlying the control of *Mesp2* expression. Tbx6 and NICD (colored ovals) interact with the conserved upstream sites in the *Mesp2* gene, sites A–D (represented by boxes). Tbx6 binds to site B (two molecules) and site D (single molecule). Site A and site C interact with RBPJκ to achieve a significant increase in *Mesp2* expression levels in the presence of Notch signals (*A*). This activation fully depends on the binding of Tbx6 to site B or site D (*B*). Tbx6 may activate *Mesp2* expression without site A and site C, presumably through an RBPJκ-independent Notch signaling pathway and via other signals (*C*). (*D*) Schematic representation of a proposed model that may explain developmentally regulated *Mesp2* expression in the anterior PSM. (*a*) NICD is highly accumulated in the anterior PSM and less in the posterior (1, 2) to activate *Mesp2* expression (red arrows). There may be a threshold level of NICD accumulation to initiate *Mesp2* activation (broken line). (*b*) Tbx6 protein is distributed in the tailbud and PSM (20) and facilitates *Mesp2* activation by NICD. (*c*) It is possible that the activation of *Mesp2* expression in the tailbud and posterior PSM, if any, is repressed by other factor(s), such as Fgf8 (36), via an unknown mechanism. (*d*) As a result, *Mesp2* expression is restricted in the anterior PSM (red box).

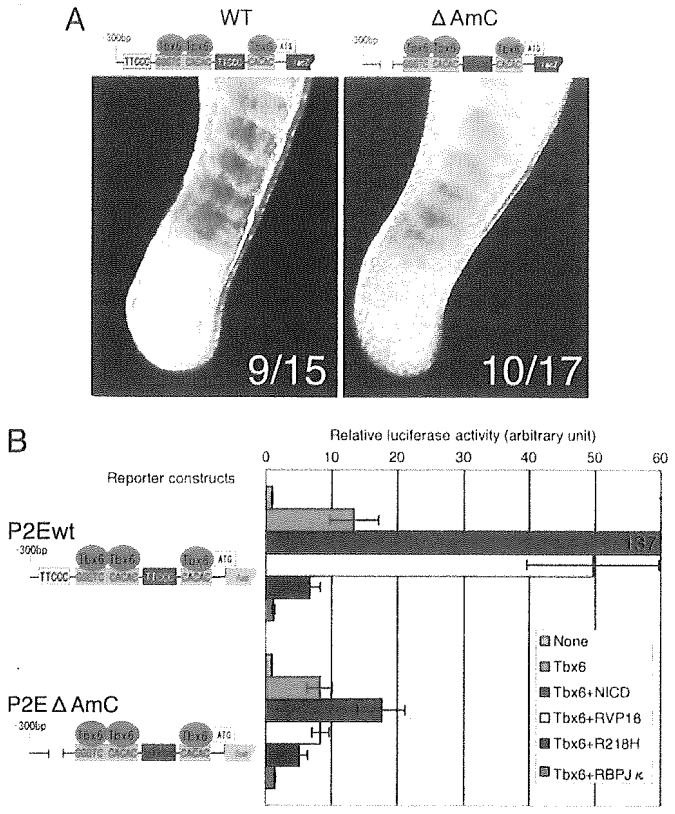

Fig. 5. The expression of *Mesp2* is not achieved solely by RBPJκ-dependent Notch signaling. (*A*) Transgenic analyses reveal that somite-specific reporter expression can still be observed by using the P2EΔAmC construct, which contains a deletion of site A and mutations in site C. The numbers of β-gal-positive embryos are indicated for each image (β-gal-positive/transgene-positive). (*B*) The expression of a dominant-negative RBPJκ diminishes reporter activation by Tbx6 for both the wild-type (wt) and P2EΔAmC (Tbx6 + R218H, purple bars) vectors. Wild-type RBPJκ also strongly suppressed reporter activity driven by Tbx6 (Tbx6+RBPJκ, orange bars). Error bars represent the standard deviation in six independent experiments.

Tbx6 itself has only weak transactivation properties, if any, and needs to cooperate with other signals such as Notch for full activity. We speculate that reporter activation by Tbx6 itself (Figs. 3 and 5) may be accomplished by cooperation with Notch signaling, presumably driven by endogenous NICD in cultured cells. Endogenous NICD concentration in cells or tissues is very low and biochemically undetectable (32). However, cultured fibroblast cells express mature Notch protein (33) and show γ-secretase-like activity that generates NICD from Notch protein (32). Furthermore, NICD activates *Hes1* reporter at very low concentrations, below the level of biochemical detection (32). Consistent with these data, *Hes1* reporter showed higher basal activity than *Mesp2* reporters or control reporter with no promoter/enhancer: 100 times higher in COS-7 cells and 60 times higher in NIH/3T3 cells in our observation (data not shown). We suppose that endogenous NICD affects the expression of Notch downstream genes in cultured cells.

NICD accumulation is observed as a strong band-like pattern in the anterior PSM and as a weak diffused signal in the posterior PSM (1, 2). Mesp2 is initially detectable in the middle of a distinct band of NICD in the anterior PSM (2), consistent with the importance of Notch signaling in *Mesp2* expression indicated by our present study. However, the weak Notch signaling activity observed in the posterior PSM may activate *Mesp2* expression, whereas *Mesp2* transcripts appear only in the anterior PSM. One possibility is that there is a "threshold" of NICD levels that is required to trigger Tbx6-dependent *Mesp2* activation (Fig. 4*D*). Because RBPJκ is expressed ubiquitously in the developing embryo (34) and strongly represses Tbx6-dependent activation of the *Mesp2* reporters (Fig. 5*B*), it may also function as a suppressor in the posterior PSM that prevents inadequate expression of *Mesp2*.

Recent reports also indicate that there are two gradients of mutually inhibitory signals, Fgf8 and RA, that have important roles in the positional determination of segment formation (35). It is likely therefore that the Fgf8 and RA signals also participate in the regulation of *Mesp2* expression. Recently, Delfini *et al.* (36) reported an intriguing result suggesting that Fgf signaling represses *Mesp* expression. Using *in ovo* electroporation, they demonstrated that the up-regulation of Fgf in the PSM diminishes the endogenous expression of *cMeso*, the chick *Mesp* homolog. It is plausible therefore that Fgf8, which is strongly expressed in the tailbud and posterior PSM, prevents the inadequate expression of *Mesp2* in posterior region. The involvement of RA in *Mesp2* expression remains elusive, however, because the disruption of *CYP26* (37), a degradation enzyme for RA, does not severely affect *Mesp2* expression levels (2). In the zebrafish embryo, FGF signaling up-regulates a basic helix–loop–helix transcription factor, her13.2, which maintains the oscillation of the Notch signals in both the tailbud and PSM by repressing the Notch-regulated genes *her1* and *her7* (38). RA and Fgf signals may thus contribute to the positioning of *Mesp2* expression by coordinating the regular oscillation of Notch signals in the tailbud and PSM.

Interestingly, it has been revealed that *Tbx6* is one of the direct targets of RBPJκ-dependent Notch signaling (39). During somitogenesis, Notch signals may first activate *Tbx6* expression in the tailbud and posterior PSM region and then activate *Mesp2* expression in the anterior PSM in cooperation with Tbx6. Furthermore, Tbx6 also works upstream of the Notch signaling pathway. In embryos of *Tbx6* hypomorphic mutant mice, *Dll1* expression in the tailbud and posterior PSM is greatly reduced (40). Promoter analyses of *Dll1* have demonstrated that Tbx6, in synergy with Wnt signaling, activates *Dll1* expression by binding to T-binding consensus sequences (20, 41). Taken together, our present results demonstrate that Tbx6 and Notch signaling constitute a regulatory network that controls somite formation via the regulation of *Mesp2* expression.

Materials and Methods

Transgenic Analyses. DNA fragments, with and without mutations in conserved upstream sites, were generated from a *Mesp2* genomic fragment by using a standard PCR-based protocol. Transgene inserts were digested from the corresponding plasmids, purified, and injected into the male pronucleus of a fertilized egg (42). The injected embryos were then transferred into pseudopregnant recipients and allowed to develop until 9.5–10.5 days postcoitum. Embryos were then analyzed for lacZ expression by X-gal staining (43) and subsequently examined for the presence of the transgene by PCR analysis (44).

Yeast One-Hybrid Screening. Synthetic oligonucleotides corresponding to contiguous sequences of conserved site A (nucleotides −199 to −191 from first ATG of *Mesp2* ORF) and site B (nucleotides −162 to −140) were inserted into the vectors pHISi-1 and placZi (Clontech), immediately upstream of the HIS3 and lacZ reporter genes, respectively. The resulting constructs were then linearized and introduced simultaneously into *Saccharomyces cerevisiae* YM4271 (Clontech) to generate the bait strain. The bait strain was then transformed by using 80 μg of 11.5 days postcoitum mouse tail cDNA library plasmid (45) to screen up to 2 million independent clones. We obtained hundreds of positive clones (HIS3+ and LacZ+) and recovered

DEVELOPMENTAL

library plasmid from 77 of these. Fifty-one of these 77 clones were sequenced and found to encode Tbx6.

EMSA. The full-length Tbx6 ORF was obtained from the pACT-Tbx6 construct, which was isolated from the yeast one-hybrid screening. After ligation to a 3XFLAG tag (Sigma), the tagged Tbx6 insert was cloned into pCS2+ (46). *In vitro* transcription/translation was then performed with a TNT *in vitro* translation kit (Promega) following the manufacturer's protocol. Oligonucleotide probes were labeled with digoxigenin-11-dideoxy UTP by using recombinant TdT (Roche Diagnostics). Crude *in vitro* translated product (5 μl) was subjected to EMSA as a protein sample. As a negative control, reticulocyte lysate without Tbx6 template was used. EMSA was performed by using the DIG Gel Shift Kit, 2nd Generation (Roche Diagnostics), following the manufacturer's protocol. The band shifts were detected by using LumiImager LAS-1000 (Fuji).

Luciferase Assay. Segments (356 bp) corresponding to the 5′-adjoining sequence of the *Mesp2* ORF, with and without mutations in the conserved binding sites, were subcloned into the pGL3-Basic (Promega) vector to generate luciferase reporter constructs. The expression vectors for the proteins to be assessed were constructed in the same way as that used in the EMSAs described above. COS-7 cells were routinely and regularly passaged in DMEM supplemented with 10% FBS. Cells were seeded at 2.5×10^4 cells per well in 24-well plates, and, after 24 h of cultivation, they were transfected with a total of 350 ng of DNA containing the reporter plasmids and expression vectors for the proteins under analysis (50 ng of each expression vector and 200 ng of reporter construct, adjusted to 350 ng by the addition of empty vector). Twenty-four hours after transfection, the cells were lysed by Passive Lysis Buffer (Promega) and subjected to a luciferase assay by using the Dual Luciferase System (Promega). In all experiments, 5 ng of the sea pansy luciferase expression vector phRL-TK (Promega) was used per well as the internal control. Luciferase activity was normalized to the phRL-TK internal control activity (sea pansy luciferase). The experiments were performed in triplicate for each assay and repeated at least twice.

We are grateful to Tasuku Honjo (Kyoto University, Kyoto) for providing cDNA clones of RBPJκ, RBPJκ-VP16, and dnRBPJκ (R218H) and to Mariko Ikumi, Eriko Ikeno, and Shinobu Watanabe for technical assistance. We also thank Hiroyuki Takeda, Mitsuru Morimoto, and Masayuki Oginuma for helpful discussions and for their comments on the manuscript. This work was supported by the Organized Research Combination System of the Ministry of Education, Culture, Sports, Science, and Technology, Japan.

1. Huppert, S. S., Ilagan, M. X., De Strooper, B. & Kopan, R. (2005) *Dev. Cell* **8,** 677–688.
2. Morimoto, M., Takahashi, Y., Endo, M. & Saga, Y. (2005) *Nature* **435,** 354–359.
3. Bessho, Y., Hirata, H., Masamizu, Y. & Kageyama, R. (2003) *Genes Dev.* **17,** 1451–1456.
4. Aulehla, A., Wehrle, C., Brand-Saberi, B., Kemler, R., Gossler, A., Kanzler, B. & Herrmann, B. G. (2003) *Dev. Cell* **4,** 395–406.
5. Sawada, A., Shinya, M., Jiang, Y. J., Kawakami, A., Kuroiwa, A. & Takeda, H. (2001) *Development* **128,** 4873–4880.
6. Moreno, T. A. & Kintner, C. (2004) *Dev. Cell* **6,** 205–218.
7. Chapman, D. L. & Papaioannou, V. E. (1998) *Nature* **391,** 695–697.
8. Saga, Y., Hata, N., Koseki, H. & Taketo, M. M. (1997) *Genes Dev.* **11,** 1827–1839.
9. Takahashi, Y., Koizumi, K., Takagi, A., Kitajima, S., Inoue, T., Koseki, H. & Saga, Y. (2000) *Nat. Genet.* **25,** 390–396.
10. Takahashi, Y., Inoue, T., Gossler, A. & Saga, Y. (2003) *Development* **130,** 4259–4268.
11. Haraguchi, S., Kitajima, S., Takagi, A., Takeda, H., Inoue, T. & Saga, Y. (2001) *Mech. Dev.* **108,** 59–69.
12. Conlon, F. L., Fairclough, L., Price, B. M., Casey, E. S. & Smith, J. C. (2001) *Development* **128,** 3749–3758.
13. Mitani, Y., Takahashi, H. & Satoh, N. (2001) *Development* **128,** 3717–3728.
14. Muller, C. W. & Herrmann, B. G. (1997) *Nature* **389,** 884–888.
15. Wilson, V. & Conlon, F. L. (2002) *Genome Biol.* **3,** REVIEWS3008.
16. Kraus, F., Haenig, B. & Kispert, A. (2001) *Mech. Dev.* **100,** 83–86.
17. Koseki, H., Wallin, J., Wilting, J., Mizutani, Y., Kispert, A., Ebensperger, C., Herrmann, B. G., Christ, B. & Balling, R. (1993) *Development* **119,** 649–660.
18. Hurlin, P. J., Steingrimsson, E., Copeland, N. G., Jenkins, N. A. & Eisenman, R. N. (1999) *EMBO J.* **18,** 7019–7028.
19. Lardelli, M. (2003) *Dev. Genes Evol.* **213,** 519–522.
20. White, P. H. & Chapman, D. L. (2005) *Genesis* **42,** 193–202.
21. Nikaido, M., Kawakami, A., Sawada, A., Furutani-Seiki, M., Takeda, H. & Araki, K. (2002) *Nat. Genet.* **31,** 195–199.
22. Davidson, B., Shi, W. & Levine, M. (2005) *Development* **132,** 4811–4818.
23. Chapman, D. L., Agulnik, I., Hancock, S., Silver, L. M. & Papaioannou, V. E. (1996) *Dev. Biol.* **180,** 534–542.
24. Mumm, J. S. & Kopan, R. (2000) *Dev. Biol.* **228,** 151–165.
25. Furriols, M. & Bray, S. (2000) *Dev. Biol.* **227,** 520–532.
26. Jarriault, S., Brou, C., Logeat, F., Schroeter, E. H., Kopan, R. & Israel, A. (1995) *Nature* **377,** 355–358.
27. Barolo, S., Walker, R. G., Polyanovsky, A. D., Freschi, G., Keil, T. & Posakony, J. W. (2000) *Cell* **103,** 957–969.
28. Matsuno, K., Go, M. J., Sun, X., Eastman, D. S. & Artavanis-Tsakonas, S. (1997) *Development* **124,** 4265–4273.
29. Hori, K., Fostier, M., Ito, M., Fuwa, T. J., Go, M. J., Okano, H., Baron, M. & Matsuno, K. (2004) *Development* **131,** 5527–5537.
30. Koizumi, K., Nakajima, M., Yuasa, S., Saga, Y., Sakai, T., Kuriyama, T., Shirasawa, T. & Koseki, H. (2001) *Development* **128,** 1391–1402.
31. Kato, H., Taniguchi, Y., Kurooka, H., Minoguchi, S., Sakai, T., Nomura-Okazaki, S., Tamura, K. & Honjo, T. (1997) *Development* **124,** 4133–4141.
32. Schroeter, E. H., Kisslinger, J. A. & Kopan, R. (1998) *Nature* **393,** 382–386.
33. De Strooper, B., Annaert, W., Cupers, P., Saftig, P., Craessaerts, K., Mumm, J. S., Schroeter, E. H., Schrijvers, V., Wolfe, M. S., Ray, W. J., *et al.* (1999) *Nature* **398,** 518–522.
34. Oka, C., Nakano, T., Wakeham, A., de la Pompa, J. L., Mori, C., Sakai, T., Okazaki, S., Kawaichi, M., Shiota, K., Mak, T. W. & Honjo, T. (1995) *Development* **121,** 3291–3301.
35. Dubrulle, J. & Pourquie, O. (2004) *Development* **131,** 5783–5793.
36. Delfini, M. C., Dubrulle, J., Malapert, P., Chal, J. & Pourquie, O. (2005) *Proc. Natl. Acad. Sci. USA* **102,** 11343–11348.
37. Sakai, Y., Meno, C., Fujii, H., Nishino, J., Shiratori, H., Saijoh, Y., Rossant, J. & Hamada, H. (2001) *Genes Dev.* **15,** 213–225.
38. Kawamura, A., Koshida, S., Hijikata, H., Sakaguchi, T., Kondoh, H. & Takada, S. (2005) *Genes Dev.* **19,** 1156–1161.
39. White, P. H., Farkas, D. R. & Chapman, D. L. (2005) *Genesis* **42,** 61–70.
40. White, P. H., Farkas, D. R., McFadden, E. E. & Chapman, D. L. (2003) *Development* **130,** 1681–1690.
41. Hofmann, M., Schuster-Gossler, K., Watabe-Rudolph, M., Aulehla, A., Herrmann, B. G. & Gossler, A. (2004) *Genes Dev.* **18,** 2712–2717.
42. Hogan, B., Beddington, R., Costantini, F. & Lacy, E. (1994) *Manipulating the Mouse Embryo: A Laboratory Manual* (Cold Spring Harbor Lab. Press, Woodbury, NY).
43. Saga, Y., Yagi, T., Ikawa, Y., Sakakura, T. & Aizawa, S. (1992) *Genes Dev.* **6,** 1821–1831.
44. Sasaki, H. & Hogan, B. L. (1996) *Genes Cells* **1,** 59–72.
45. Ohara, O., Nagase, T., Mitsui, G., Kohga, H., Kikuno, R., Hiraoka, S., Takahashi, Y., Kitajima, S., Saga, Y. & Koseki, H. (2002) *DNA Res.* **9,** 47–57.
46. Rupp, R. A., Snider, L. & Weintraub, H. (1994) *Genes Dev.* **8,** 1311–1323.

DEVELOPMENTAL DYNAMICS 235:395–402, 2006

RESEARCH ARTICLE

Mesp1-Nonexpressing Cells Contribute to the Ventricular Cardiac Conduction System†

Satoshi Kitajima,[1]* Sachiko Miyagawa-Tomita,[2] Tohru Inoue,[3] Jun Kanno,[1] and Yumiko Saga[4]*

Previous fate mapping analysis, using Cre recombinase driven by the *Mesp1* locus, revealed that *Mesp1* is expressed in almost all of the precursors of the cardiovascular system, including the endothelium, endocardium, myocardium, and epicardium. *Mesp1*-nonexpressing cells were found to be restricted to the outflow tract cushion and along the interventricular septum (IVS), which is a location that is suggestive of specialized cardiac conduction system (CCS). In our current study, we examined the identity of these IVS cells by using the pattern of β-galactosidase activity in *CCS-lacZ* mice. In addition, by crossing *Mesp1-Cre* and *floxed GFP reporter* mice with *CCS-lacZ* mice, we have calculated that approximately 20% of the ventricular CCS within the IVS corresponds to *Mesp1*-nonexpressing cells. These data suggest that the ventricular CCS is of heterocellular origin. Furthermore, we indicate a possibility that a population of the cells that contribute to the ventricular CCS might be distinguished at an early stage of development. *Developmental Dynamics 235:395–402, 2006.* © 2005 Wiley-Liss, Inc.

Key words: *Mesp1*; mesoderm; heart differentiation; cardiac conduction system; cell-lineage analysis

Accepted 30 September 2005

INTRODUCTION

The heart is the first functional organ to be formed during organogenesis, and cells that are destined to form cardiac mesoderm are induced both before and during gastrulation. The cells of the cardiac mesoderm invaginate through the primitive streak and migrate with the cranial mesoderm. The bilaterally symmetric cardiac precursors subsequently migrate and converge at the midline of the embryo to form the cardiac crescent, which then forms a linear, single heart tube. The heart tube, formed by an outer myocardium and an inner endocardium, then undergoes rightward looping, which is lined by an acellular matrix (the cardiac jelly). The looped heart tube then undergoes septation to generate a mature, four-chambered cardiac structure in mammals.

The heart is composed of three major cardiac cell types: (1) the endocardium, a part of which forms the cushion tissue by transformation from epithelial to mesenchymal cells; (2) the myocardium; and (3) the epicardium (for review, see Moorman and Christoffels, 2003). The major components of the heart, such as endocardium and myocardium, are of mesodermal origin (i.e., cardiogenic mesoderm), but the contribution of other cell lineages has also been reported for both chick and mouse. Fate mapping of the avian cardiac neural crest has been well documented, and it was reported previously from such

The Supplementary Material referred to in this article can be found at http://www.interscience.wiley.com/jpages/1058-8388/suppmat

† This article was accepted for inclusion in Developmental Dynamics 235#1, January 2006—Cardiovascular Special Issue.

[1] Division of Cellular & Molecular Toxicology, Biological Safety Research Center, National Institute of Health Sciences, Setagaya-ku, Tokyo, Japan
[2]Department of Pediatric Cardiology, The Heart Institute of Japan, Tokyo Women's Medical University, Shinjuku-ku, Tokyo, Japan
[3]Biological Safety Research Center, National Institute of Health Sciences, Setagaya-ku, Tokyo, Japan
[4]Division of Mammalian Development, National Institute of Genetics, Mishima, Japan

Grant sponsor: Ministry of Education, Science, Sports, and Culture in Japan; Grant sponsor: Burroughs–Wellcome Fund Clinical Scientist Award in Translational Research.

***Correspondence to: Yumiko Saga, Ph.D., Division of Mammalian Development, National Institute of Genetics, Yata 1111, Mishima 411-8540, Japan. E-mail: ysaga@lab.nig.ac.jp or Satoshi Kitajima, D.V.M.Ph.D, Division of Cellular & Molecular Toxicology National Institute of Health Sciences, 1-18-1 Kamiyohga, Setagaya-ku, Tokyo 158-8501, Japan. E-mail: satoshi@nihs.go.jp**

DOI 10.1002/dvdy.20640
Published online 29 November 2005 in Wiley InterScience (www.interscience.wiley.com).

experiments using quail–chick chimera that two types of mesenchyme, cardiac neural crest derived and non-neural crest derived, participate in outflow septation and remodeling (Kirby et al., 1983; Waldo et al., 1998). Recently, through the use of the Cre-*loxP* system in mice, it has been demonstrated clearly that the cardiac outflow tract (OT) cushions are contributed in part by cardiac neural crest cells (Yamauchi et al., 1999; Jiang et al., 2000). Additionally, lineage analysis using *Tie2-cre* in mice has suggested that the OT cushions are of mixed origins, containing neural crest cells and endocardium, whereas the atrioventricular (AV) cushions are mainly derived from cells originating from endocardium (Kisanuki et al., 2001).

The specialized cardiac conduction system (CCS) includes the sinoatrial (SA) node, which generates a pacemaker impulse; the AV node, which delays the electrical impulse and allows for the sequential contraction of the atrial and ventricular chambers of the heart; and the ventricular CCS, such as the atrioventricular bundle (AVB), bundle branches, and their ramifications, which facilitates the fast and coordinated conduction of impulses to and throughout the ventricles. Cells in the CCS are characterized by their larger size, reduced number of myofibrils, and large accumulations of glycogen (Mikawa, 1999). It has also been suggested that the CCS might be categorized into two parts based on their origin (Moorman et al., 1998, 2003). One is the SA and AV nodes, which might be derived from the slow-conducting myocardium of the inflow tract and AV canal. The other one is the ventricular CCS, which possibly develops from the trabecular ventricular component. In chick, an elegant series of experiments using retroviral lineage-tracing has provided strong evidence that ventricular components of the conduction system are derived from cardiomyogenic cells (Gourdie et al., 1995; Cheng et al., 1999). In addition, it has been suggested that the differentiation of a subset of Purkinje fibers, adjacent to the arterial bed, might be regulated by local signals from the coronary artery (Gourdie et al., 1995). It was subsequently shown that endothelin-1, a paracrine factor secreted by endothelial cells, is capable of inducing embryonic chick myocytes to the cells of the CCS.

In contrast to the avian CCS, the ventricular CCS in most mammals is morphologically and topologically different from that of chick as it is mainly subendocardial. Hence, the developmental role of the coronary artery in mammalian CCS differentiation is uncertain. In the murine heart, the expression of several markers, including specific connexins and *lacZ* under the transcriptional regulation of either the *minK* or *HF-1b* loci, delineate the bundle branches and proximal Purkinje fibers, but none appear to delineate the full extent of the conductive network along the ventricular free walls (Delorme et al., 1995; Coppen et al., 1998, 1999; Kupershmidt et al., 1999; Nguyen-Tran et al., 2000). In contrast, the entire mouse CCS, including the distal Purkinje fiber network, in both embryonic and neonatal hearts has been visualized recently by way of β-galactosidase (β-gal) reporter activity (Rentschler et al., 2001) in the *CCS-lacZ* mouse line. Recently, the β-gal–positive cells in the interventricular septum (IVS) region of the *CCS-lacZ* adult mice have been reported to correspond to the Cx40-positive cells (Myers and Fishman, 2004). However, the comparison was performed by using serial sections; thus, further clarification is needed to determine whether the same cell expresses the both markers or not. Nevertheless, it is considered that the β-gal–positive cells of *CCS-lacZ* embryos are the most reliable indication for CCS cells in the mouse embryo, compared with the other markers. Although the lineage of the cells of the murine CCS is incompletely characterized, a recent study demonstrated that exogenous treatment of 8.5–10.5 days postcoitum (dpc) embryos with neuregulin-1, an endocardial-derived growth and differentiation factor essential for ventricular trabeculation, could induce a CCS-like phenotype in embryonic cardiomyocytes (Rentschler et al., 2002). Whereas, the use of in vitro culture systems has demonstrated also that the treatment of embryonic stem cells with endothelin-1 but not with neuregulin-1 increased the percentage of pacemaker-like cells, suggesting that the role of endothelin-1 in CCS development may be conserved, even in mice (Gassanov et al., 2004).

Mesp1 and Mesp2 are transcription factors that contain almost identical basic helix–loop–helix (bHLH) motifs and are encoded by genes that both localize in chromosome 7 (Saga et al., 1996, 1997). Disruption of the *Mesp1* gene results in cardia bifida (Saga, 1998). We also have shown previously, using double knockout mouse embryos and by chimera analysis, that *Mesp1* and *Mesp2* are essential for the development of cardiac mesoderm (Kitajima et al., 2000). *Mesp1* expression is restricted to the nascent mesodermal cells, and its expression is transient and down-regulated before heart tube formation (Saga et al., 1999). However, lineage analysis using *Mesp1-cre* has revealed that *Mesp1*-expressing cells are incorporated into almost all of the precursors of the cardiovascular system (i.e., endothelium, endocardium, myocardium, and epicardium), both in embryonic and extraembryonic regions at 9.5 dpc, and that *Mesp1* expression is the earliest detectable molecular marker in heart precursor cells (Saga et al., 1999, 2000). In this current study, we describe further detailed lineage analyses of the mouse heart using *Mesp1-cre* mice. We show that *Mesp1*-nonexpressing cells contribute to neural crest-derived regions as well as to a subset of the cells in the ventricular CCS.

RESULTS

Lineage Analysis of *Mesp1*-Expressing Mesodermal Cells in the Developing Heart

Using *Mesp1-cre*–mediated cell lineage analysis, we previously reported that *Mesp1*-expressing cells were incorporated into almost all precursors of the cardiovascular system in both embryonic and extraembryonic regions at 9.5 dpc (Saga et al., 2000). However, further analysis at 13.5 dpc now has revealed that the cardiogenic cells are not entirely contributed by *Mesp1*-expressing cells, suggesting that the origin of these cells may be subdivided according to *Mesp1* expression (Fig. 1A–C). At this developmen-

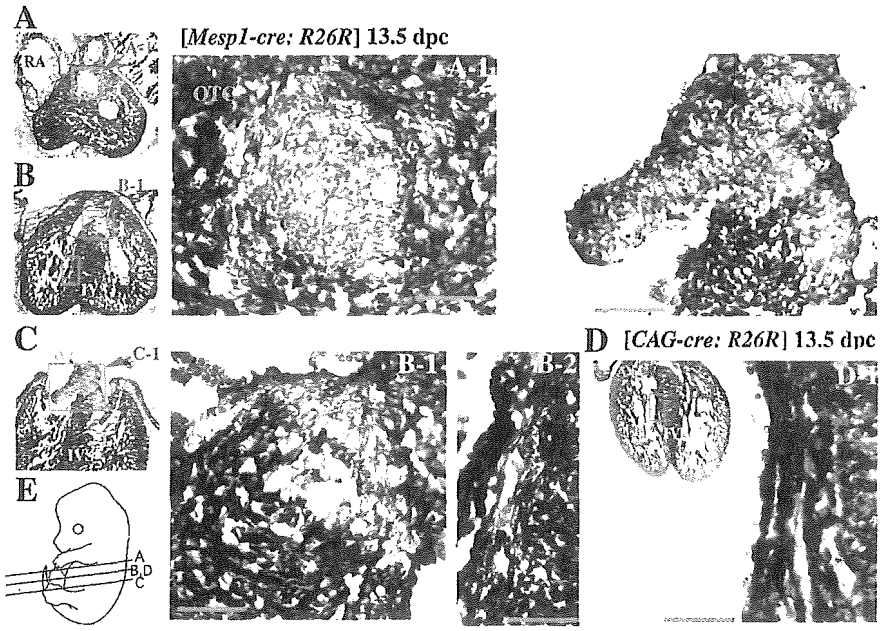

Fig. 1. Transverse sections of β-galactosidase (β-gal) -stained *Mesp1-cre:R26R* or *CAG-cre: R26R* embryos at 13.5 days post coitum (dpc). **A–B:** The β-gal–negative areas were observed in the region of outflow tract cushions (OTC; A; boxed area in A-1) and along the interventricular septum (IVS) in a pattern reminiscent of the ventricular cardiac conduction system (CCS; B; boxed areas, B-1 and B-2). **C:** atrioventricular cushions (AVC; boxed area in C-1) showed β-gal activity. Original magnification, ×100. Magnified images of OT cushion cells, the interventricular regions, and AV cushions are shown in A-1, B-1 and -2, and C-1, respectively. **D:** Transverse sections of β-gal–stained *CAG-cre:R26R* embryos show no β-gal–negative regions, suggesting that *R26R* expression was not shut down as *Mesp1*-nonexpressing cells differentiate. A magnified image in the interventricular regions is shown in D-1. **E:** Sectioning planes are illustrated and were counterstained with eosin. LV, left ventricle; RA, right atrium; RV, right ventricle. Scale bar = 100 μm.

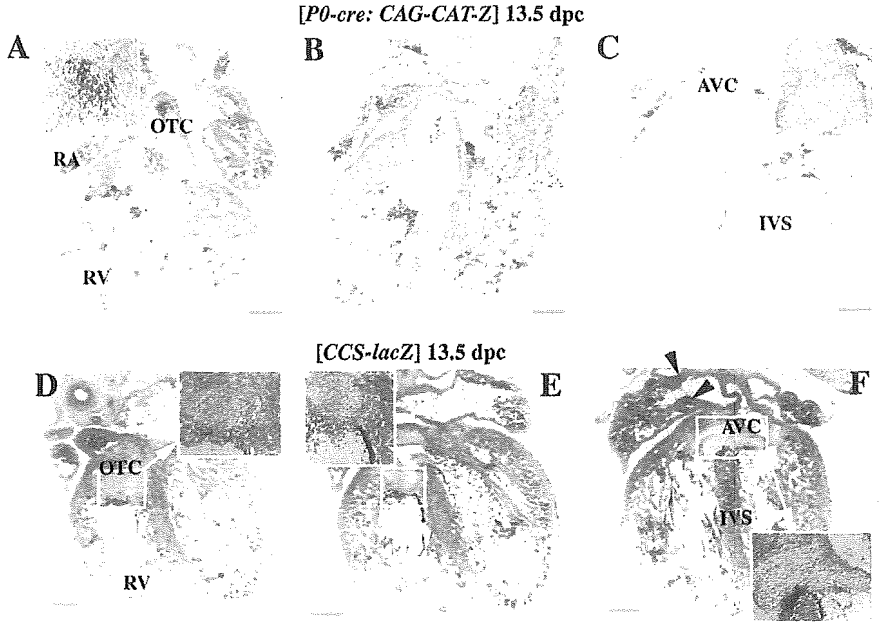

Fig. 2. β-galactosidase (β-gal) staining in sections of the *P0-cre:CAG-CAT-Z* and the *CCS-lacZ* embryos at 13.5 days post coitum (dpc). **A–C:** In the *P0-cre:CAG-CAT-Z* embryo, high β-gal activity is observed in the region of the outflow tract cushion (OTC; A, boxed area), but little activity is evident in the region of the atrioventricular cushion (AVC; C, boxed area). Original magnification, ×40. Note that the β-gal activity was not observed within the ventricle and the interventricular septum (IVS; B). **D–F:** The images in the boxed area are magnified. In the *CCS-lacZ* embryo, β-gal activity is observed strongly in part of the atria (indicated by arrowheads) and along the IVS in a pattern reminiscent of the ventricular cardiac conduction system (CCS; boxed area). In contrast, β-gal activity in either the OTC or AVC regions was barely detectable (D,F). The images in the boxed area are magnified. Sectioning planes of images A–C and D–F are the same as those illustrated in Figure 1E: A–C, respectively. All sections were counterstained with eosin. RA, right atrium; RV, right ventricle. Scale bar = 200 μm.

tal stage (13.5 dpc), during which the septation complexes start to form, *Mesp1*-nonexpressing cells are also visible along the IVS region in a pattern reminiscent of the AVB and bundle branches, which are components of the ventricular CCS (Fig. 1B). In addition, region of the OT cushions had little β-gal activity (Fig. 1A), unlike most of the AV cushions that had strong activity (Fig. 1C). In the *CAG-cre* mouse, in which the *cre* gene is under the control of the cytomegalovirus immediate early enhancer-chicken beta-actin hybrid (*CAG*) enhancer, it has been reported that the sequence between the two *loxP* sites is deleted in all tissues in the mouse embryo (Sakai and Miyazaki, 1997). This finding was confirmed in our current experiments; all of the cells in the developing heart of double-transgenic embryos were positive for *LacZ* (Fig. 1D), indicating that this expression is not down-regulated upon *CAG* promoter activation. This observation strongly suggests that *Mesp1*-"non" expressing cells are indeed present in the developing murine heart of the *Mesp1-cre:R26R* reporter double-transgenic mouse.

Because neural crest cells are known to contribute to part of the developing heart structure (Jiang et al., 2000), we initially expected that the regions containing *Mesp1*-nonexpressing cells might reflect this population. To address this possibility more fully, we next compared our findings with a previous report that used a *P0-cre* transgene and *CAG-CAT-Z* reporter gene to identify neural crest-derived cells (Yamauchi et al, 1999).

Mesp1-Nonexpressing Cells Along the Ventricular Septum Are Not Derived From the Neural Crest

We analyzed *P0-cre:CAG-CAT-Z* embryos to examine whether neural crest cells indeed contribute to any of the regions occupied by *Mesp1*-nonexpressing cells. In the *P0-cre:CAG-CAT-Z* embryo at 13.5 dpc, β-gal activity was mainly detected in the mesenchyme located within the OT cushions of the heart (Fig. 2A), which is consistent with previous findings (Yamauchi et al., 1999) and a report using *Wnt1-cre* mice (Jiang et al.,

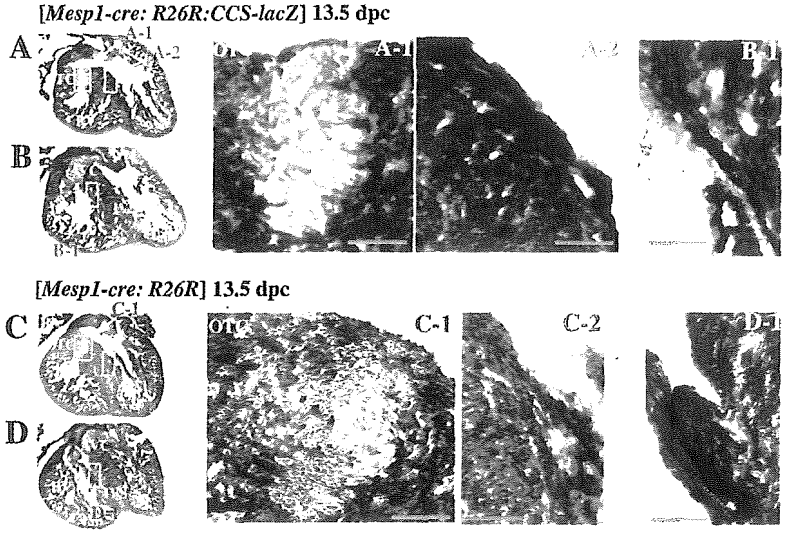

Fig. 3.

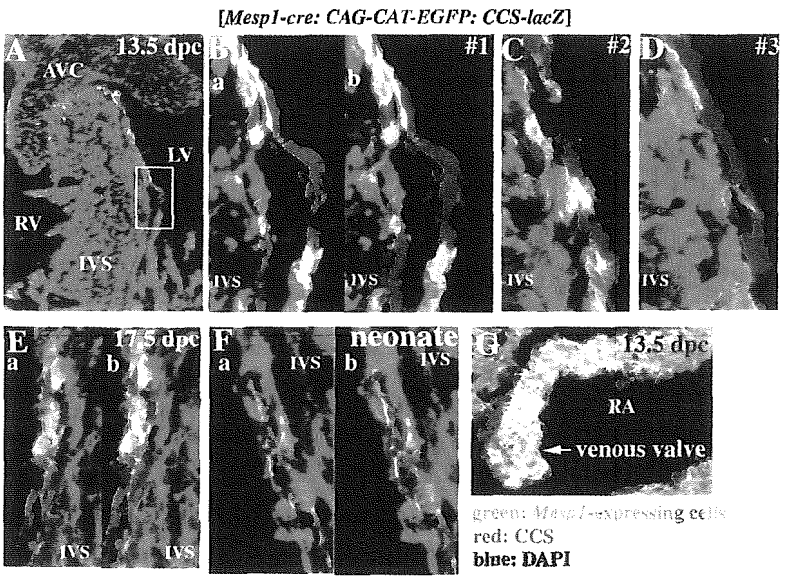

Fig. 4.

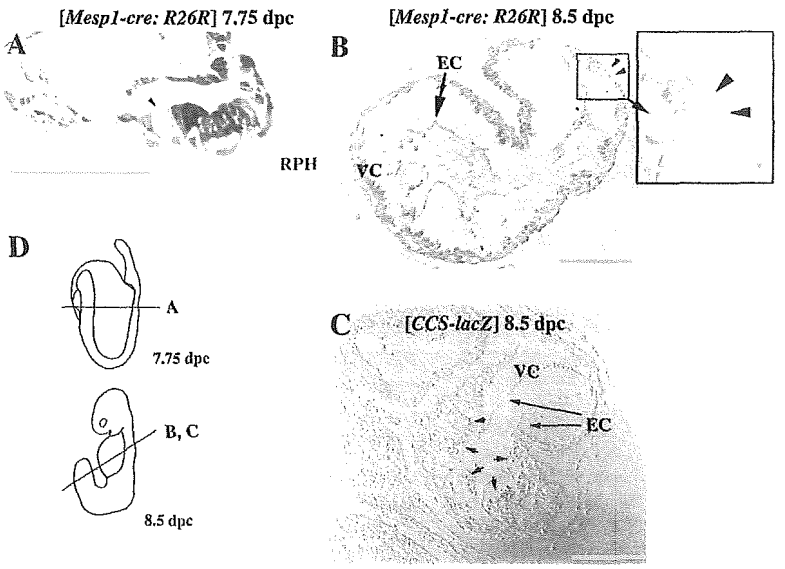

Fig. 5.

Fig. 3. Comparison of β-gal staining patterns between *Mesp1-cre:R26R:CCS-lacZ* triple hetero-embryos and *Mesp1-cre:R26R* embryos. **A,B:** Sections of the heart of the *Mesp1-cre:R26R:CCS-lacZ* embryo at 13.5 days post coitum (dpc). **C,D:** Compared with the *Mesp1-cre:R26R* embryo (boxes in C-2 and D-1), *Mesp1*-nonexpressing cells along the interventricular (IVS) were barely observed in the *Mesp1-cre:R26R:CCS-lacZ* triple hetero-embryos (A,B; boxes in A-2 and B-1). However, *Mesp1*-nonexpressing cells in outflow tract (OT) cushion regions were also detected, even in the triple hetero-embryos (box A-1). Original magnification, ×100. The images in the boxed area are magnified. Sectioning planes of A, B, and C, D are the same as those illustrated in Figure 1E: B and C, respectively. Sections were counterstained with eosin. AVC, atrioventricular cushion; IVS, interventricular septum; RA, right atrium; RV, right ventricle; Scale bar = 100 μm.

Fig. 4. *Mesp1*-nonexpressing cells contribute to a subset of the ventricular cardiac conduction system (CCS). Triple immunostaining for *Mesp1*-expressing cells (green fluorescent protein [GFP] -positive cells; green), cells of the ventricular CCS (LacZ-positive cells; red), and nuclei (4′,6′-diamidino-2-phenylindole [DAPI] staining; blue) in a *Mesp1-cre:CAG-CAT-EGFP:CCS-lacZ* embryo. All images shown are merged views, and double immunostaining of GFP and LacZ (a) and a triple immunostaining image with additional DAPI staining (b) are shown in some cases. **A–D:** A merged view of the interventricular (IVS) region at 13.5 days post coitum (dpc). The boxed area of the ventricular CCS in A was magnified as shown in B. Other sections derived from additional embryos are shown in C and D. The presence of red cells suggests that *Mesp1*-nonexpressing cells actually belong to the ventricular CCS, whereas some *Mesp1*-expressing cells also colocalize here (yellow). Typical images of mixed cell populations are shown in B and C, whereas a red cell-dominant section is shown in D. Original magnification, ×400, except for A, which is ×100. **E,F:** Merged view in the IVS region in an embryo at 17.5 dpc (E) or in a neonate (F). Original magnification, ×400. Red cells (i.e., the *Mesp1*-nonexpressing cells belonging to the CCS) were observed even at later stages beyond 13.5 dpc. **G:** The region of the venous valves, which are proposed remnants of the embryonic sinoatrial (SA) ring, at 13.5 dpc. Almost all of the cells in this region were stained yellow, suggesting that the cells belonging to the venous valves are *Mesp1*-expressing. Original magnification, ×200. Sectioning planes are those between B and C, illustrated in Figure 1E. AVC, atrioventricular cushion; LV, left ventricle; OTC, outflow tract cushion; RA, right atrium; RV, right ventricle.

Fig. 5. Comparison of transverse sections of β-gal stained *Mesp1-cre:R26R* embryos with *CCS-lacZ* embryos at an earlier stage. **A:** At 7.75 days post coitum (dpc) in *Mesp1-cre:R26R* embryos, we observed a few *Mesp1*-nonexpressing cells within the primitive heart tube (arrow head). Original magnification, ×400. **B:** At 8.5 dpc, the regions of the *Mesp1*-nonexpressing cells in *Mesp1-cre:R26R* embryos, were observed more clearly (arrowheads). **C:** The β-gal–positive regions (i.e., the cells belonging to the CCS) were observed mainly in the subendocardial myocardium of 8.5 dpc *CCS-lacZ* mouse (arrows). Original magnification, ×200. **D:** Sectioning planes are illustrated. Sections were counterstained with eosin. EC, endocardium; RPH, right primitive heart tube; VC, ventricular chamber. Scale bars = 100 μm.

2000). There were only minimal contributions by neural crest cells in the AV cushions, as predicted by the β-gal activity in the *Mesp1-cre:R26R* mouse (Fig. 2C). Importantly, however, neural crest-derived mesenchyme was not observed in either part of the ventricle or the IVS (Fig. 2B), where *Mesp1*-nonexpressing cells were visible (Fig. 1B). This finding indicates that other cell types must contribute to this particular region. Intriguingly, the distribution of *Mesp1*-nonexpressing cells resembled that of the AVB and bundle branches and also the Purkinje fibers of the CCS. This prompted us to speculate that ventricular CCS cells might be derived from lineages that are distinct from both the neural crest and *Mesp1*-expressing mesodermal cells.

Mesp1-Nonexpressing Cells Contribute to the CCS

As a preliminary approach to determine whether or not *Mesp1*-nonexpressing cells did in fact reside in the CCS, we compared these cells with the β-gal expression patterns in embryonic hearts of *CCS-lacZ* transgenic mice. In these mice, the specialized CCS can be visualized by β-gal activity (Rentschler et al., 2001). In 13.5 dpc hearts from these transgenic animals, strong β-gal activity could be observed in part of the atrium, which could correspond to the SA node. This high level of activity could also be detected along the IVS, which demarcates the ventricular CCS, including the AVB and bundle branches (Fig. 2D–F). When comparing these results with those shown in Figure 1, the portion of the *Mesp1*-nonexpressing cell population along the IVS was found to show a similar pattern to the β-gal–positive regions in the *CCS-lacZ* mice, suggesting that these *Mesp1*-nonexpressing cells contribute to the ventricular CCS.

To provide direct evidence for our hypothesis that cells of the ventricular CCS are indeed derived from *Mesp1*-nonexpressing cells, we generated triple transgenic *Mesp1-cre:R26R:CCS-lacZ* mice. Because both the *CCS-lacZ* and *R26R* transgenic mice use β-gal as a marker, the entire region contributed by the *Mesp1*-nonexpressing cells in the IVS would become β-gal–positive in the triple hetero-embryonic hearts if our contention was correct. As shown in Figure 3, this was found to be the case, as all of the cells in the IVS had β-gal activity, which was in contrast to the corresponding sections of the *Mesp1-cre:R26R* embryo (Fig. 3C,D). Moreover, the region of the OT cushions had little β-gal activity even in the triple hetero-embryo (Fig. 3A), supporting our conclusion that this region is occupied mainly by cells of neural crest origin. Hence, these data suggest that the *Mesp1*-nonexpressing cells in the IVS belong to the ventricular CCS.

It was still unclear, however, whether all of the ventricular CCS is derived from *Mesp1*-nonexpressing cells, because both the *CCS-lacZ* and *R26R* reporter mice use the same β-gal marker. We, therefore, performed a similar series of studies using the *CAG-CAT-EGFP* strain (Kawamoto et al., 2000), in which GFP expression is dependent upon cre-mediated recombination and representative results are shown in Figure 4. *Mesp1*-nonexpressing cells at 13.5 dpc do indeed reside within the ventricular CCS (*Mesp1*-nonexpressing/*CCS-lacZ*-positive red cells in Fig. 4A–D), although it is clear that the CCS is also observed in the *Mesp1*-expressing cell populations (i.e., *Mesp1*-expressing/*CCS-lacZ*–positive yellow cells). In addition, after 4′,6′-diamidino-2-phenylindole (DAPI) staining, we observed that all of the green fluorescent protein (GFP) -negative *Mesp1*-nonexpressing cells belonged to the lacZ-positive cells of the ventricular CCS, because cells positive for DAPI alone (blue) were rarely observed along the IVS (b in Fig. 4A–C). To demonstrate the heterocellular origin of CCS more unequivocally and to analyze the ratios quantitatively, we generated serial sections of the embryonic heart along the anteroposterior axis and analyzed the staining patterns.

A total of three embryos were sectioned and 58 sections containing CCS-LacZ staining in the IVS region were further subjected to semiquantitative analysis (Supplementary Figure S1, which can be viewed at http://www.interscience.wiley.com/jpages/1058-8388/suppmat). However, as the CCS distributes peripherally in the IVS with multiple branchings, it is very difficult to quantify. We, therefore, roughly estimated the ratio by counting DAPI stained nuclei in each cell type and selected 28 typical sections, from which 16 showed a colocalization pattern for yellow and red cells (Fig. 4B,C). Of these 16 sections, 2 and 5 showed a red cell- and a yellow cell-dominant pattern, respectively (Fig. 4D, and data not shown). We have estimated that approximately 20% of the ventricular CCS, along the IVS, corresponds to *Mesp1*-nonexpressing cells. Moreover, red cells (i.e., the *Mesp1*-nonexpressing cells belonging to the ventricular CCS) were also observed in the ventricular CCS even at later developmental stages of 17.5 dpc (Fig. 4E) and in neonates at 4 days after birth (Fig. 4F). The AV cushion cells were weakly positive for the GFP signal, due to the thinness of the cytoplasm and resulting lower intensity of fluorescence (Fig. 4A), but their identity was confirmed by LacZ staining in *Mesp1-cre; R26R* embryos (Fig. 1C). Thus, we conclude unequivocally that the population of *Mesp1*-nonexpressing cells, which we identified along the ventricular septum, contributes to the CCS.

In the case of the SA or AV node regions of the CCS, the contribution of *Mesp1*-expressing and/or *Mesp1*-nonexpressing cells was not as clear from our present results using embryos at 13.5 dpc, because these typical node structures were not discernible. In contrast, we were able to determine that most of the cells in the venous valves, which are the proposed remnants of the embryonic SA ring in the fully developed heart (Rentschler et al., 2001), of the *Mesp1-cre:CAG-CAT-EGFP:CCS-lacZ* embryo were *Mesp1*-expressing (i.e., GFP–positive cells). This determination was revealed by the *Mesp1*-expressing/*CCS-lacZ*–positive yellow cells at 13.5 dpc (Fig. 4G). However, the developmental relationships between the venous valves and both the SA and AV nodes have not yet been determined.

Origin of *Mesp1*-Nonexpressing Cells

To determine the origin of the *Mesp1*-nonexpressing cells, we examined the *LacZ* expression profiles in more immature *Mesp1-cre:R26R* and *CCS-lacZ* embryos. As shown in Figure 5A,

even at 7.75 dpc, at which stage the cardiac crescent can be observed, a few β-gal–negative cells were detectable in the *Mesp1-cre:R26R* embryo. The β-gal–negative cells were observed in the myocardium region more clearly at 8.5 dpc (Fig. 5B). In the *CCS-lacZ* embryo, although the heart region at 7.75 dpc was confirmed to be β-gal–negative (data not shown) as reported previously (Rentschler et al., 2001), patchy staining was observed mainly in the subendocardial myocardium region at 8.5 dpc (Fig. 5C). However, a direct relationship between the *Mesp1*-nonexpressing cells and the CCS cells is still not clear, although the neural crest cells, which are also identifiable as *Mesp1*-nonexpressing cells in our system, have not yet arrived in the heart at this stage and can be excluded (Jiang et al., 2000).

DISCUSSION

In this study, we have found using a Cre-*loxP* site-specific recombination system that the origin of the cardiac mesenchyme is subdivided according to the presence of *Mesp1* expression. We demonstrate that the regions occupied by *Mesp1*-nonexpressing cells correspond to two distinct populations of cells: one derived from the neural crest and the other one that contributes to the ventricular CCS.

Comparison of the Cell-Lineages of Neural Crest Cells and *Mesp1*-Nonexpressing cells

In our experiments with *Mesp1-cre:R26R* embryos, we have found that cells derived from the neural crest are negative but that mesodermal cells derived from *Mesp1*-expressing cells are positive, for β-gal activity. We have also confirmed that mammalian cardiac neural-crest cells are *Mesp1*-negative (Figs. 1, 2) and contribute to the mesenchyme in the OT cushions of the heart. These observations were made following neural crest cell lineage analyses using the *P0-cre:CAG-CAT-Z* strain (Fig. 2) and are consistent with previous results obtained using *Wnt1-cre:R26R* double transgenic mice (Jiang et al., 2000). The origin of the cells of the AV cushions was suggested to be mesodermal, because this region was occupied by *Mesp1*-expressing cells in our study (Fig. 1C). This result is consistent with the previous study of Kisanuki et al. (2001) using *Tie2-cre* mice that reported that the origin of the AV cushions is mainly of endocardial cell lineage. Thus, mesenchymal cells in the OT cushions are derived from mainly neural crest cells and those in the AV cushions are derived from endocardium.

Importantly, we observed a second population of *Mesp1*-nonexpressing cells, along the IVS (Fig. 1B). Because this region is not contributed by neural crest cells (Fig. 2B), we explored the possibility that these *Mesp1*-nonexpressing cells reside in the ventricular CCS. Before examining this possibility, we first confirmed that the failure to express β-gal in the *Mesp1-cre:R26R* embryos was not due to an artifact, such as down-regulation of *LacZ* expression during differentiation or mosaicism of Cre recombinase expression. To exclude the former possibility, we examined *CAG-cre:R26R* mice, in which Cre recombinase is ubiquitously expressed and all cells should be *LacZ*-positive. We did not subsequently observe any *LacZ*-negative cells in the heart, indicating that there had been no down-regulation of *LacZ* upon cell differentiation (Fig. 1D). To exclude possible mosaicism of Cre recombinase, we repeated our analysis in more than 20 embryos and observed very consistent results, although some clonal differences may exist. In addition, when we crossed the *Mesp1-cre* and *CCS-lacZ* strains and monitored *R26R*-dependent reporter gene expression, we did not observe patchy *LacZ*-negative cells in the ventricular wall. Thus, it appears unlikely that mosaicism of the *R26R* reporter could account for our results.

As for the contribution of the neural crest cells into the ventricular CCS, it was reported that neural crest-derived cells were observed in the vicinity of the CCS in the IVS at 14.5 dpc using the *Wnt1-cre:R26R* reporter system (Poelmann et al., 2004). Thus, the possibility cannot be rule out that the neural crest cells contribute to CCS in the IVS, although we could not detect any β-gal–positive cells in the IVS in our *P0-cre:CAG-CAT-Z* system. The discrepancy could be due to the difference in systems used for lineage analyses. The future studies using triple transgenic strategy (*Wnt1-cre:CAG-CAT-GFP:CCS-lacZ*) as used in our current study would be useful to discriminate the discrepancy.

Origins of the CCS

Using *Mesp1-cre:R26R* embryos, we identified a population of *Mesp1*-nonexpressing cells that were found to be distributed in the wall along the ventricular septum (Fig. 1B). The results of genetic crosses with the *CCS-lacZ* strain suggested that these *Mesp1*-nonexpressing cells contribute to the ventricular CCS (Fig. 3B). To confirm these findings, we generated triple transgenic *Mesp1-cre:CAG-CAT-EGFP:CCS-lacZ* mice. Double-staining for GFP and β-gal expression and/or additional DAPI staining in these mice confirmed that the *Mesp1*-nonexpressing cells contribute approximately 20% of the ventricular CCS (Fig. 4). Moreover, these populations of cells can be distinguished at a stage as early as stage 7.75 dpc at least (Fig. 5), whereas *Mesp1* is initially, albeit transiently, expressed at 6.5 dpc (Saga et al., 1996).

The pacemaking and conduction systems of the heart are composed of the SA node, AV node, AVB, the bundle branches, and the Purkinje fibers, each of which can be distinguished morphologically, functionally, and molecularly (Moorman and Christoffels, 2003). The origin of the nodal tissue is less clear than that of the ventricular CCS, although the primary myocardium is suggested to be a candidate (Moorman and Christoffels, 2003). Recently, it was suggested that some of the working myocardium could also differentiate into nodal tissues, even after birth (Pashmforoush et al., 2004). Although the developmental relationships between the venous valves and the nodes have not yet been fully elucidated, our data indicate that most of cells in the venous valves, which are proposed to be remnants of the embryonic SA ring (Rentschler et al., 2001), are derived from *Mesp1*-expressing cells (Fig. 4G). However, further detailed studies will be required to determine the precise cellular origin of the nodes and their relationships with the venous valves.

In the present analyses, we have focused on the cell-lineages of the ventricular CCS and shown them to be of

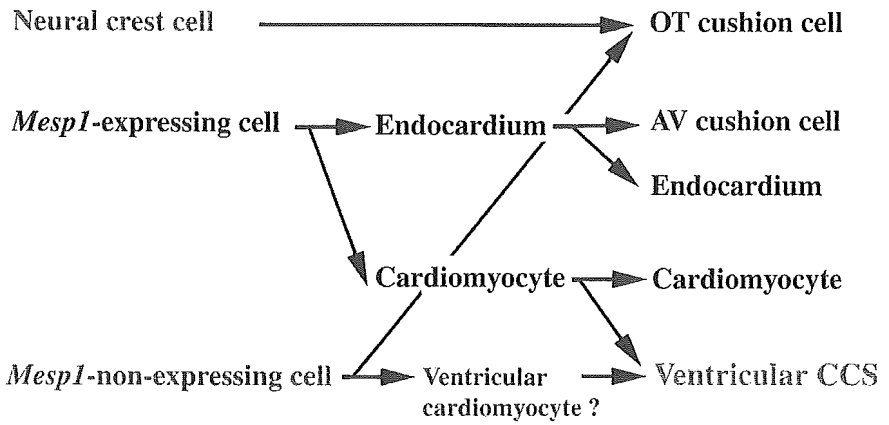

Fig. 6. Summary of the origin and cell-fate relationships of cardiac mesenchyme cell types. Each cardiac cell type is established by three distinct origins: neural crest cells, the mesodermal cells of *Mesp1*-expressing cells, and *Mesp1*-nonexpressing cells. It is noteworthy that both the *Mesp1*-expressing cells and the *Mesp1*-nonexpressing cells contribute to the ventricular CCS. In addition, the origins of the subset of the ventricular CCS that are contributed by the *Mesp1*-nonexpressing cells are distinguishable from that of the myocardium by the *Mesp1* expression profile. We speculate that the *Mesp1*-nonexpressing cardiomyocyte may be a candidate for the origin of the subset of the ventricular CCS. [Color figure can be viewed in the online issue, which is available at www.interscience.wiley.com.]

heterocellular origin. Two possibilities have emerged from both our analyses and previous reports concerning the origin of the ventricular CCS in mouse, occupied by *Mesp1*-nonexpressing cells. First, it is conceivable that the *Mesp1*-nonexpressing cells in the CCS are not derived from cardiomyocytes. Alternatively, these cells may represent cardiomyocytes, which simply do not express *Mesp1*. We favor this latter possibility. Lineage tracing experiments in chick have convincingly demonstrated that the ventricular CCS, including the Purkinje fibers, are derived from cardiomyocytes (reviewed in Mikawa, 1999; Pennisi et al., 2002). Moreover, experiments in the mouse also indicate that embryonic cardiomyocytes can be converted to a CCS-like phenotype in response to neuregulin-1, at least when assayed by up-regulation of the *CCS-lacZ* transgene (Rentschler et al., 2002). Nonetheless, additional analyses will be required to determine the basis for the molecular heterogeneity within the ventricular CCS and to determine whether there is associated functional diversity in this structure.

In conclusion, we have determined that *Mesp1*-nonexpressing cells contribute to the ventricular CCS in addition to the OT cushion. Furthermore, we indicate a possibility that a population of the cells that contribute to the ventricular CCS might be distinguished at an early stage of development. Unfortunately, it could not be clarified from our present experiments whether *Mesp1*-nonexpressing cells also contributed to the other regions of the CCS, such as the SA or AV nodes. A scheme summarizing the cell lineage relationships in the developing murine heart is shown in Figure 6. Our observation that the ventricular CCS includes both *Mesp1*-expressing and -nonexpressing cells is evidence of the heterogeneous nature of the ventricular CCS. The further identification of specific molecular markers for the mouse CCS, expressed at early embryonic stages, will undoubtedly enhance our understanding of the developmental biology of the CCS in the heart.

EXPERIMENTAL PROCEDURES

Lineage Analysis of *Mesp1*-Expressing Cells

The *Mesp1-cre* knockin mouse was constructed by introduction of a gene encoding Cre recombinase into the *Mesp1* locus, as previously described (Saga et al., 1999). The fidelity of expression was confirmed by in situ hybridization at E7.0 (data not shown). Genotyping was performed by polymerase chain reaction using a neo-specific primer NeoAL2: 5′-GGGGATGCGGTGGGCTCTATGGCTT-3′ and *Mesp1* primer MesP1-GR1: 5′-ATATGCCAAGTCATTGAGGTGAGCTTTC-3′. *Mesp1-cre* mice were crossed with either *CAG-CAT-Z* (Araki et al., 1995), *R26R* (Soriano, 1999), or *CAG-CAT-EGFP* (Kawamoto et al., 2000) reporter mice. *P0-cre* (Yamauchi et al., 1999) and *CCS-lacZ* mice (Rentschler et al., 2001) were also used for cell lineage analyses. Mice were maintained on a 7:00 AM to 7:00 PM light–dark cycle, with noon on the day of vaginal plug discovery defined as 0.5 dpc.

β-gal Staining, Immunostaining, and In Situ Hybridization

Embryos that had been fixed at 7.5–10.5 dpc were stained for the detection of β-galactosidase activity in whole-mounts as described previously (Saga et al., 1992). The specimens were then dehydrated by means of a graded ethanol series, embedded in either paraffin wax or plastic resin (technovit 8100, Heraeus Kulzer, Inc.) and sectioned at a thickness of 4 μm. Hearts that had been isolated from embryos at later stages were subjected to β-gal staining after sectioning. Briefly, hearts were fixed in a solution of 2% paraformaldehyde, 0.05% glutaraldehyde, and 0.02% NP-40 in phosphate buffer (PBS) for 30 min on ice. The tissues were then sequentially soaked in a graded series of 10, 20, and 30% sucrose (w/v) in PBS while being gently agitated on a shaking platform, culminating in a 50:50 mix of 30% sucrose:OCT. Samples were frozen and stored at −80°C until sectioning at 8 μm thickness, and the sections were placed on gelatin-coated slides. Frozen sections of *Mesp1-cre:CAG-CAT-EGFP:CCS-lacZ* mouse hearts was stained with anti-lacZ and anti-GFP antibodies as follows: sections prepared were fixed with 4% paraformaldehyde for 3 min, treated with 10 μg/ml proteinase K and blocked in 3% skim milk for 30 min at room temperature (RT). Blocking solutions was replaced with rabbit anti–β-gal antibody (Cappel, ICN Pharmaceuticals, Inc., OH) at a dilution of 1:2,000 and with rat anti-GFP antibody (Nacalai Tesque, Kyoto, Japan) at a dilution 1:200 and incubated overnight at 4°C. After brief washes in PBS, the sections were incubated with Alexa 594–conjugated anti-rabbit followed by Alexa 488–conjugated anti-rat secondary antibodies at dilutions of 1:200

for 90 min at RT. These sections were then incubated with 0.1 μg/ml of DAPI (Sigma, St. Louis, MO) for 5 min to visualize nuclei.

ACKNOWLEDGMENTS

We thank the following researchers for providing mice: Dr. Jun-ichi Miyazaki (*CAG-cre*, *CAG-CAT-Z*, and *CAG-CAT-EGFP*), Dr. Kuniya Abe (*P0-cre*), Dr. Philippe Soriano (*R26R*), and Dr. Glenn I. Fishman (*CCS-lacZ*). We also thank Seiko Shinzawa, Mariko Ikumi, Eriko Ikeno, Chizuko Obata, Shinobu Watanabe, and Maho Endo for technical assistance.

REFERENCES

Araki K, Araki M, Miyazaki J, Vassalli P. 1995. Site specific recombination of a transgene in fertilized eggs by transient expression of Cre recombinase. Proc Natl Acad Sci U S A 92:160–164.

Cheng G, Litchenberg WH, Cole GJ, Mikawa T, Thompson RP, Gourdie RG. 1999. Development of the cardiac conduction system involves recruitment within a multipotent cardiomyogenic lineage. Development 126:5041–5049.

Coppen SR, Dupont E, Rothery S, Severs NJ. 1998. Connexin45 expression is preferentially associated with the ventricular conduction system in mouse and rat heart. Circ Res 82:232–243.

Coppen SR, Severs NJ, Gourdie RG. 1999. Connexin45 (alpha 6) expression delineates an extended conduction system in the embryonic and mature rodent heart. Dev Genet 24:82–90.

Delorme B, Dahl E, Jarry-Guichard T, Marics I, Briand JP, Willecke K, Gros D, Theveniau-Ruissy M. 1995. Developmental regulation of connexin 40 gene expression in mouse heart correlates with the differentiation of the conduction system. Dev Dyn 204:358–371.

Gassanov N, Er F, Zagidullin N, Hoppe UC. 2004. Endothelin induces differentiation of ANP-EGFP expressing embryonic stem cells towards a pacemaker phenotype. FASEB J 18:1710–1712.

Gourdie RG, Mima T, Thompson RP, Mikawa T. 1995. Terminal diversification of the myocyte lineage generates Purkinje fibers of the cardiac conduction system. Development 121:1423–1431.

Jiang X, Rowitch DH, Soriano P, McMahon AP, Sucov HM. 2000. Fate of the mammalian cardiac neural crest. Development 127:1607–1616.

Kawamoto S, Niwa H, Tashiro F, Sano S, Kondoh G, Takeda J, Tabayashi K, Miyazaki J. 2000. A novel reporter mouse strain that expresses enhanced green fluorescent protein upon Cre-mediated recombination. FEBS Lett 470: 263–268.

Kirby ML, Gale TF, Stewart DE. 1983. Neural crest cells contribute to normal aorticopulmonary septation. Science 220: 1059–1061.

Kisanuki YY, Hammer RE, Miyazaki J, Williams SC, Richardson JA, Yanagisawa M. 2001. Tie2-Cre transgenic mice: a new model for endothelial cell-lineage analysis in vivo. Dev Biol 230:230–242.

Kitajima S, Takagi A, Inoue T, Saga Y. 2000. MesP1 and MesP2 are essential for the development of cardiac mesoderm. Development 127:3215–3226.

Kupershmidt S, Yang T, Anderson ME, Wessels A, Niswender KD, Magnuson MA, Roden DM. 1999. Replacement by homologous recombination of the minK gene with lacZ reveals restriction of minK expression to the mouse cardiac conduction system. Circ Res 84:146–152.

Mikawa T. 1999. Cardiac lineages. In: Harvey RP, Rosenthal N, editors. Heart development. San Diego: Academic Press. p 19–33.

Moorman AFM, Christoffels VM. 2003. Cardiac chamber formation: development, genes, and evolution. Physiol Rev 83:1223–1267.

Moorman AFM, deJong F, Denyn MM, Lamers WH. 1998. Development of the cardiac conduction system. Circ Res 82: 629–644.

Myers DC, Fishman GI. 2004. Toward an understanding of the genetics of murine cardiac pacemaking and conduction system development. Anat Rec A Discov Mol Cell Evol Biol 280:1018–1021.

Nguyen-Tran VT, Kubalak SW, Minamisawa S, Fiset C, Wollert KC, Brown AB, Ruiz-Lozano P, Barrere-Lemaire S, Kondo R, Norman LW, et al. 2000. A novel genetic pathway for sudden cardiac death via defects in the transition between ventricular and conduction system cell lineages. Cell 102:671–682.

Pashmforoush M, Lu JT, Chen H, Amand TS, Kondo R, Pradervand S, Evans SM, Clark B, Feramisco JR, Giles W, Ho SY, Benson DW, Silberbach M, Shou W, Chien KR. 2004. Nkx2–5 pathways and congenital heart disease; loss of ventricular myocyte lineage specification leads to progressive cardiomyopathy and complete heart block. Cell 117:373–386.

Pennisi DJ, Rentschler S, Gourdie RG, Fishman GI, Mikawa T. 2002. Induction and patterning of the cardiac conduction system. Int J Dev Biol 46:765–775.

Poelmann RE, Jongbloed MR, Molin DG, Fekkes ML, Wang Z, Fishman GI, Doetschman T, Azhar M, Gittenberger-de Groot AC. 2004. The neural crest is contiguous with the cardiac conduction system in the mouse embryo: a role in induction? Anat Embryol (Berl) 208:389–393.

Rentschler S, Vaidya DM, Tamaddon H, Degenhardt K, Sassoon D, Morley GE, Jalife J, Fishman GI. 2001. Visualization and functional characterization of the developing murine cardiac conduction system. Development 128:1785–1792.

Rentschler S, Zander J, Meyers K, France D, Levine R, Porter G, Rivkees SA, Morley GE, Fishman GI. 2002. Neuregulin-1 promotes formation of the murine cardiac conduction system. Proc Natl Acad Sci U S A 99:10464–10469.

Saga Y. 1998. Genetic rescue of segmentation defect in MesP2-deficient mice by MesP1 gene replacement. Mech Dev 75: 53–66.

Saga Y, Yagi T, Ikawa Y, Sakakura T, Aizawa S. 1992. Mice develop normally without tenascin. Genes Dev 6:1821–1831.

Saga Y, Hata N, Kobayashi S, Magnuson T, Seldin M, Taketo MM. 1996. MesP1: a novel basic helix-loop-helix protein expressed in the nascent mesodermal cells during mouse gastrulation. Development 122:2769–2778.

Saga Y, Hata N, Koseki H, Taketo MM. 1997. Mesp2: a novel mouse gene expressed in the presegmented mesoderm and essential for segmentation initiation. Genes Dev 11:1827–1839.

Saga Y, Miyagawa-Tomita S, Takagi A, Kitajima S, Miyazaki J, Inoue T. 1999. MesP1 is expressed in the heart precursor cells and required for the formation of a single heart tube. Development 126: 3437–3447.

Saga Y, Kitajima S, Miyagawa-Tomita S. 2000. *Mesp1* expression is the earliest sign of cardiovascular development. Trends Cardiovasc Med 10:345–352.

Sakai K, Miyazaki J. 1997. A transgenic mouse line that retains Cre recombinase activity in mature oocytes irrespective of the cre transgene transmission. Biochem Biophys Res Commun 237:318–324.

Soriano P. 1999. Generalized lacZ expression with the ROSA26 Cre reporter strain. Nat Genet 21:70–71.

Waldo K, Miyagawa-Tomita S, Kumiski D, Kirby ML. 1998. Cardiac neural crest cells provide new insight into septation of the cardiac outflow tract: aortic sac to ventricular septal closure. Dev Biol 196: 129–144.

Yamauchi Y, Abe K, Mantani A, Hitoshi Y, Suzuki M, Osuzu F, Kuratani S, Yamamura K. 1999. A novel transgenic technique that allows specific marking of the neural crest cell lineage in mice. Dev Biol 212:191–203.

Differential contributions of Mesp1 and Mesp2 to the epithelialization and rostro-caudal patterning of somites

Yu Takahashi[1,*], Satoshi Kitajima[1], Tohru Inoue[1], Jun Kanno[1] and Yumiko Saga[2,*]

[1]Cellular & Molecular Toxicology Division, National Institute of Health Sciences, 1-18-1 Kamiyoga, Setagayaku, Tokyo 158-8501, Japan
[2]Division of Mammalian Development, National Institute of Genetics, Yata 1111, Mishima 411-8540, Japan
*Authors for correspondence (e-mail: yutak@nihs.go.jp and ysaga@lab.nig.ac.jp)

Accepted 29 November 2004

Development 132, 787-796
Published by The Company of Biologists 2005
doi:10.1242/dev.01597

Summary

Mesp1 and Mesp2 are homologous basic helix-loop-helix (bHLH) transcription factors that are co-expressed in the anterior presomitic mesoderm (PSM) just prior to somite formation. Analysis of possible functional redundancy of Mesp1 and Mesp2 has been prevented by the early developmental arrest of Mesp1/Mesp2 double-null embryos. Here we performed chimera analysis, using either Mesp2-null cells or Mesp1/Mesp2 double-null cells, to clarify (1) possible functional redundancy and the relative contributions of both Mesp1 and Mesp2 to somitogenesis and (2) the level of cell autonomy of Mesp functions for several aspects of somitogenesis. Both Mesp2-null and Mesp1/Mesp2 double-null cells failed to form initial segment borders or to acquire rostral properties, confirming that the contribution of Mesp1 is minor during these events. By contrast, Mesp1/Mesp2 double-null cells contributed to neither epithelial somite nor dermomyotome formation, whereas Mesp2-null cells partially contributed to incomplete somites and the dermomyotome. This indicates that Mesp1 has a significant role in the epithelialization of somitic mesoderm. We found that the roles of the Mesp genes in epithelialization and in the establishment of rostral properties are cell autonomous. However, we also show that epithelial somite formation, with normal rostro-caudal patterning, by wild-type cells was severely disrupted by the presence of Mesp mutant cells, demonstrating non-cell autonomous effects and supporting our previous hypothesis that Mesp2 is responsible for the rostro-caudal patterning process itself in the anterior PSM, via cellular interaction.

Key words: Somitogenesis, Epithelial-mesenchymal conversion, Mesp2, Chimera analysis, Mouse

Introduction

Somitogenesis is not only an attractive example of metameric pattern formation but is also a good model system for the study of morphogenesis, particularly epithelial-mesenchymal interconversion in vertebrate embryos (Gossler and Hrabe de Angelis, 1997; Pourquié, 2001). The primitive streak, or tailbud mesenchyme, supplies the unsegmented paraxial mesoderm, known as presomitic mesoderm (PSM). Mesenchymal cells in the PSM undergo mesenchymal-epithelial conversion to form epithelial somites in a spatially and temporally coordinated manner. Somites then differentiate, in accordance with environmental cues from the surrounding tissues, into dorsal epithelial dermomyotome and ventral mesenchymal sclerotome (Borycki and Emerson, 2000; Fan and Tessier Lavigne, 1994). Hence, the series of events that occur during somitogenesis provide a valuable example of epithelial-mesenchymal conversion. The dermomyotome gives rise to both dermis and skeletal muscle, whereas the sclerotome forms cartilage and bone in both the vertebrae and the ribs. Each somite is subdivided into two compartments, the rostral (anterior) and caudal (posterior) halves. This rostro-caudal polarity appears to be established just prior to somite formation (Saga and Takeda, 2001).

Mesp1 and Mesp2 are closely related members of the basic helix-loop-helix (bHLH) family of transcription factors but share significant sequence homology only in their bHLH regions (Saga et al., 1996; Saga et al., 1997). During development of the mouse embryo, both *Mesp1* and *Mesp2* are specifically expressed in the early mesoderm just after gastrulation and in the paraxial mesoderm during somitogenesis. Mesp1/Mesp2 double-null embryos show defects in early mesodermal migration and thus fail to form most of the embryonic mesoderm, leading to developmental arrest (Kitajima et al., 2000). Mesp1-null embryos exhibit defects in single heart tube formation, due to a delay in mesodermal migration, but survive to the somitogenesis stage (Saga et al., 1999), suggesting that there is some functional redundancy, i.e. compensatory functions of Mesp2 in early mesoderm. During somitogenesis, both *Mesp1* and *Mesp2* are expressed in the anterior PSM just prior to somite formation. Although we have shown that Mesp2, but not Mesp1, is essential for somite formation and the rostro-caudal patterning of somites (Saga et al., 1997), a possible functional redundancy between Mesp1 and Mesp2 has not yet been clearly established.

To further clarify the contributions of Mesp1 and Mesp2 to somitogenesis, analysis of Mesp1/Mesp2 double-null embryos